Provenance of the Surveyor Fan and Precursor Sediments in the Gulf of Alaska—Implications of a Combined U-Pb, (U-Th)/He, Hf, and Rare Earth Element Study of Detrital Zircons

Barbara Huber,[1,*] *Heinrich Bahlburg,*[1] *Jasper Berndt,*[2] *István Dunkl,*[3] *and Axel Gerdes*[4]

1. Institute of Geology and Palaeontology, Westfälische Wilhelms-Universität, Münster, Germany; 2. Institute of Mineralogy, Westfälische Wilhelms-Universität, Münster, Germany; 3. Institute of Sedimentology and Environmental Geology, Georg-August University, Göttingen, Germany; 4. ICPMS Lab, Institute of Geosciences, Goethe University, Frankfurt, Germany

ABSTRACT

The history of exhumation and denudation of the Cenozoic St. Elias orogen is stored in the sediments of the Miocene to Holocene Surveyor Fan, Gulf of Alaska. The orogeny of the mountain belt coincides with major climatic events leading to varying degrees of glaciation that are considered to have strongly interacted with mountain-building processes. In order to assess the relative influence of climate and tectonics on erosion patterns and to reconstruct sediment routing to the ocean, we combine zircon U-Pb dating and (U-Th)/He thermochronology with analysis of rare earth elements and Hf isotopes of zircons of sands and silts from Integrated Ocean Drilling Program expedition 341 sites U1417 and U1418 in the Surveyor Fan. All Miocene to Pleistocene sediments show similar U-Pb age spectra, indicating that the main source areas remained the same during different stages of glaciation. A prominent age component at 50–60 Ma can be linked to the Chugach Metamorphic Complex and the Sanak-Baranof plutonic belt in the mountain range. Older grains can be referred to low-grade metamorphic sources within the Chugach, Prince William, and Yakutat terranes. A decrease in 50–60 Ma igneous and metamorphic zircons implies a reduction of input from the Chugach Metamorphic Complex and the Sanak-Baranof plutonic belt. This indicates that the southward advance of glaciers toward the ocean, together with tectonic changes from the Miocene to the Pliocene, triggered a higher contribution from the newly glaciated areas. During times of increased glaciation in the Pleistocene, glaciers appear to have been nested in the same area as before. Our data do not give evidence of a general change in the drainage systems or the tectonic setting during the Pleistocene but also do not prove the absence of such.

Online enhancements: appendix, supplemental tables.

Introduction

Erosional mass transfer intimately links the evolution of orogenic topography to the deposition in periorogenic basins. In the case of the Neogene to Quaternary St. Elias orogen at the southern Alaska margin, tectonically induced exhumation is modulated by climate processes triggering varying degrees and styles of glaciation (e.g., Berger et al. 2008*a*, 2008*b*; Enkelmann et al. 2008, 2010, 2017; Gulick et al. 2015; Falkowski and Enkelmann 2016; Worthington et al. 2018). The formation of the St. Elias orogen is caused by northwestward movement of the Yakutat terrane along the Fairweather strike-slip fault toward the Pamplona Zone and the Aleutian Trench and collision along the Chugach–St. Elias fault (fig. 1). Exhumation in the orogen has been found to vary in time and space. An area of extremely rapid exhumation has been identified (the St. Elias syntaxis) that has been moving to the south since ca. 10 Ma (late Miocene), and different exhumation scenarios have been suggested for the Pleistocene (e.g., Berger et al. 2008*a*; Enkelmann et al. 2008, 2009, 2010, 2015, 2017; Spotila and Berger 2010; Falkowski et al. 2014; Worthington et al. 2018).

Manuscript received November 24, 2017; accepted June 26, 2018; electronically published September 19, 2018.
* Author for correspondence; email: barbara.huber@uni-muenster.de.

[The Journal of Geology, 2018, volume 126, p. 000–000] © 2018 by The University of Chicago.
All rights reserved. 0022-1376/2018/12606-0002$15.00. DOI: 10.1086/699740

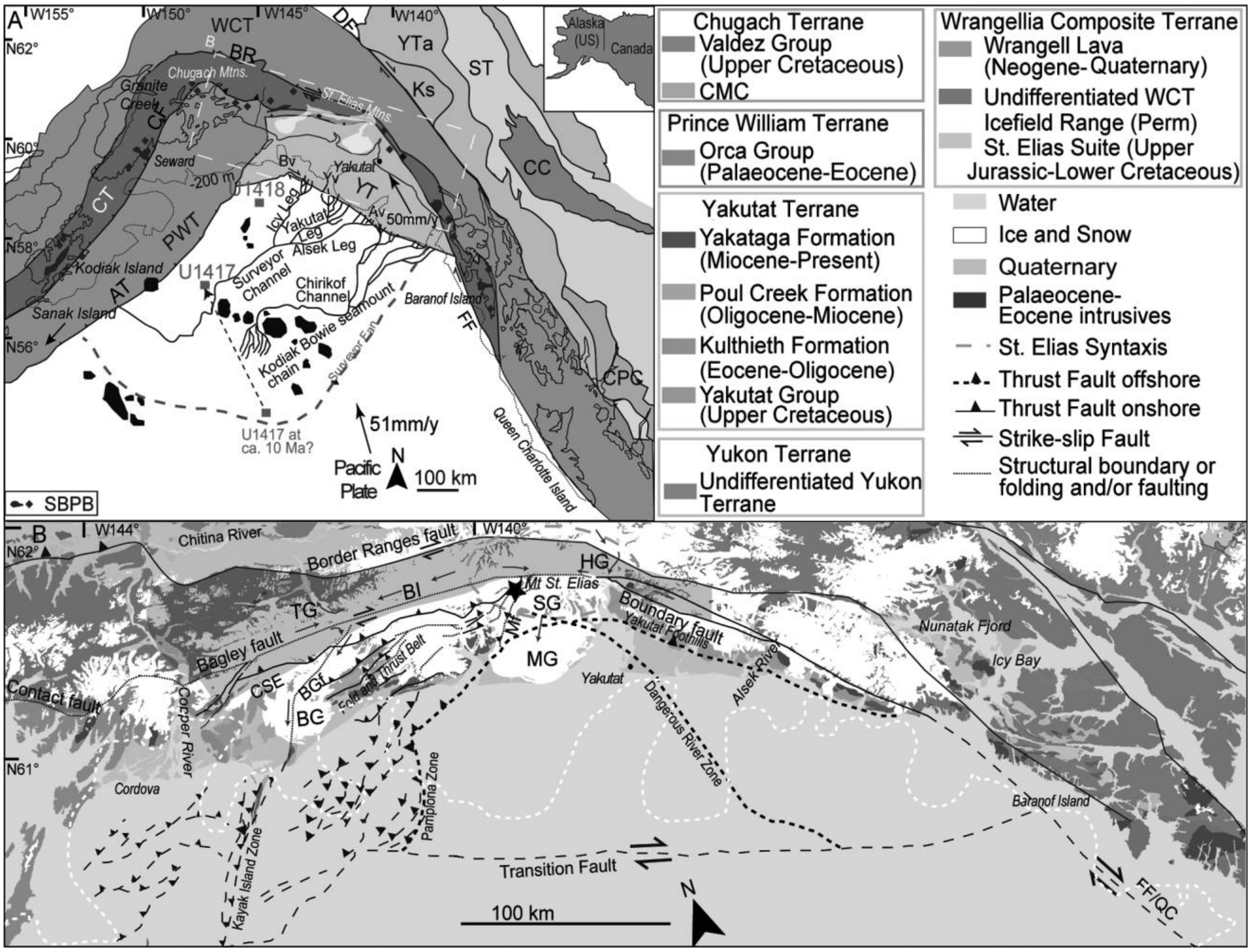

Figure 1. *A*, Terrane map of the southern Alaska continental margin. Squares mark the distal (U1417) and proximal (U1418) sites of Integrated Ocean Drilling Program (IODP) Expedition 341. The dashed arrow indicates the roughly estimated position of sampling site U1417 at ca. 10 Ma and its movement to its present position. AT = Aleutian Trench; Av = Alsek valley; BR = Border Ranges fault; Bv = Bering valley; CC = Cache Creek terrane; CF = Contact fault; CPC = Coast Plutonic Complex; CT = Chugach terrane; KS = Kluane schist; FF = Fairweather fault; PWT = Prince William terrane; SBPB = Sanak-Baranof plutonic belt; ST = Stikinia terrane; WCT = Wrangellia composite terrane; YT = Yakutat terrane; YTa = Yukon-Tana terrane; Yv = Yakutat valley. *B*, Simplified geological map of the southern Alaska continental margin. Arrows indicate glacial flow directions, after Post (1972). Glacier extent during the Last Glacial Maximum, after Manley and Kaufman (2002), is marked with a dashed white line. The extent of the Chugach Metamorphic Complex (CMC) is marked by the gray shaded area south of the Border Ranges fault. Modified after Huber et al. (2018) and references therein. BG = Bering glacier; BGf = Bering glacier fault; BI = Bagley icefield; CSE = Chugach–St. Elias fault; FF/QC = Queen Charlotte–Fairweather fault system; HG = Hubbard glacier; Mf = Malaspina fault; MG = Malaspina glacier; SG = Seward glacier; TG = Tana glacier. A color version of this figure is available online.

In the course of the St. Elias orogeny, alpine glaciation began at the southern Alaska continental margin in the late Miocene (ca. 7 Ma) and increased to tidewater glaciation at the Miocene/Pliocene boundary (ca. 6.7–5.0 Ma; glacial interval A in fig. 3; Lagoe et al. 1993). After a warm period in the middle Pliocene (glacial interval B; Lagoe et al. 1993), glaciers returned during the Pleistocene. This coincided with a change in global glacial-interglacial climate cycles from 40 to 100 ka at the mid-Pleistocene transition (MPT; ca. 0.7–1 Ma), which caused an increase in glaciation and the establishment of highly erosive ice streams (glacial interval C; Lagoe and Zellers 1996). The impact of these changes in glacial intensity on and their interaction with ongoing tectonic processes are still poorly understood, partly because glaciers still cover wide parts of the orogen (e.g., Spotila et al. 2004; Berger et al. 2008*a*; Berger and Spotila 2008; Meigs et al. 2008;

Enkelmann et al. 2010, 2015, 2017; Spotila and Berger 2010; Worthington et al. 2010, 2018; Expedition 341 Scientists 2014; Gulick et al. 2015).

As the windward side of the orogen faces the Gulf of Alaska, the major part of the detrital mass export from the orogen to the ocean ends up as deep-sea sediments on the Gulf of Alaska abyssal plain, in particular in the Surveyor deep-sea fan (Stevenson and Embley 1987; Berger et al. 2008*a*, 2008*b*; Reece et al. 2011; Gulick et al. 2015). Sediments on the Gulf of Alaska abyssal plain range in age from early Miocene to Holocene. They record the exhumation of the St. Elias Mountains and reflect the interaction of tectonic and climatic processes governing the terrigenous mass transfer to the abyssal plain (Ingle 1973; Plafker 1987; Plafker et al. 1994; Reece et al. 2011; Jaeger et al. 2014; Gulick et al. 2015; Montelli et al. 2017).

Previous studies of zircon and apatite U-Pb and fission-track (FT) double-dating and heavy-mineral analysis of sediments from the Surveyor Fan and precursor sediments revealed the usefulness of these sediments to constrain information on onshore exhumation rates during the Miocene to Pliocene and provenance (Dunn et al. 2017; Huber et al. 2018). In this contribution, we present new detrital zircon data on the geochemical composition, U-Pb age distributions, Hf isotope patterns, and (U-Th)/He thermochronological data of Miocene through Pleistocene sediments from two sites drilled by Integrated Ocean Drilling Program (IODP) Expedition 341 on the distal and proximal Surveyor Fan (sites U147 and U1418, respectively; fig. 1*A*). Each detrital zircon grain stores a variety of information on the temporal evolution and geochemistry of its source rock (Gehrels et al. 2014), which is conducive to constraining the catchment of the recovered sediments.

Background

Geology. The southernmost part of the southern Alaska margin formed through accretion of several terranes against the Yukon composite terrane (Yukon-Tanana, Stikine, and Cache Creek terranes). These are, from north to south, the Wrangellia composite terrane, the Chugach–Prince William terrane, and the Yakutat terrane (fig. 1*A*; Plafker 1987). The Wrangellia composite terrane was emplaced against the continental margin in mid-Cretaceous time and consists of Paleozoic and Mesozoic magmatic-arc assemblages (Plafker et al. 1994). The Chugach and Prince William terranes were accreted during the Middle to Late Cretaceous and host a complex deformed accretionary belt (Plafker 1987; Plafker et al. 1994). Wide parts are made up of the flysch of the Upper Cretaceous Valdez Group (depositional age of 99–60 Ma), while the Orca Group (depositional age 69 to ~35 Ma) makes up most of the Prince William terrane (fig. 1*B*; Mendenhall 1905; Dumoulin 1987; Plafker et al. 1994). The partially ice-covered Contact fault separates the two terranes. Eocene ridge subduction resulted in the emplacement of plutons of the Sanak-Baranof plutonic belt (SBPB), a 2100-km-long belt of granodioritic and granitic plutons that intruded into the active accretionary prism between Sanak and Baranof Islands (intrusion ages of ca. 61 Ma in the west and ca. 50 Ma in the east; fig. 2), and formation of the Chugach Metamorphic Complex (CMC; Sisson et al. 1989, 2003; Bradley et al. 1993, 2003; Plafker et al. 1994; Pavlis and Sisson 1995; Haeussler et al. 2003; Farris and Paterson 2009). The CMC is a metamorphic complex of up to amphibolite facies metamorphic grade that spans a distance of ca. 350 km along strike of the orogen (Hudson and Plafker 1982; Bruand et al. 2011; Gasser et al. 2011).

The currently accreting and subducting Yakutat terrane is bordered by the Kayak Island Zone in the west and by the Chugach–St. Elias and Fairweather–Queen Charlotte faults in the north and east. The Transition fault separates it from the Pacific plate in the south. Northwestward movement of the Yakutat terrane along the dextral Fairweather–Queen Charlotte transform fault system started at ca. 30 Ma (Plafker 1987). Two different scenarios have been suggested for the transport history of the Yakutat terrane. The far-traveled options suggests an origin close to northern California or southern Oregon in the Eocene (~45 Ma; Bruns 1983; Plafker et al. 1994), requiring ca. 1500–2000 km, or ca. 24°, of northward transport (Perry et al. 2009; White et al. 2017). The short-traveled option suggests transport over a relatively short distance, starting ca. 600 km to the southeast (near Prince Rupert; Plafker 1987; Plafker et al. 1994; Perry et al. 2009). Since ca. 6 Ma, the Yakutat terrane and the Pacific plate have both moved in a northwestward direction at ca. 50 mm/y relative to the North American plate (Elliott et al. 2010; Gulick et al. 2015).

Flat-slab subduction of the Yakutat terrane since the Oligocene and collision with the North American plate along the Chugach–Saint Elias fault system since the Miocene resulted in the formation of the St. Elias Mountains (Plafker et al. 1994; Enkelmann et al. 2008, 2015; Finzel et al. 2011; Arkle et al. 2013; Falkowski et al. 2014). About 600 km of the Yakutat terrane has already been subducted (fig. 1*A*; Plafker et al. 1994; Eberhart-Phillips et al. 2006; Fuis et al. 2008; Finzel et al. 2011; Worthington et al. 2012). Very high exhumation rates have been found in the

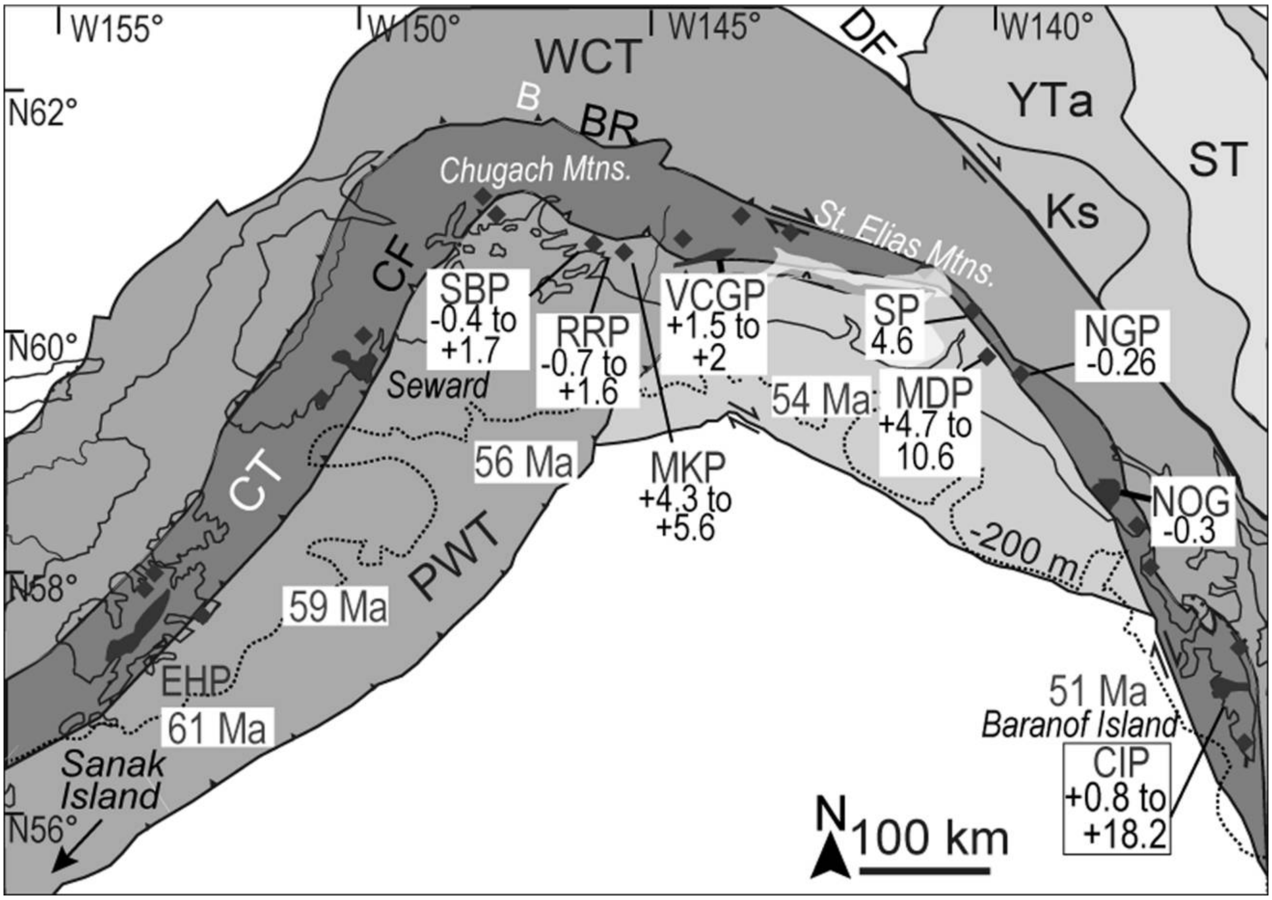

Figure 2. Simplified terrane map of southern Alaska, modified after Carlson et al. (1996), Colpron et al. (2007), Colpron and Nelson (2011), and Grabowski et al. (2013), with U-Pb ages of the intrusions from the Sanak-Baranof plutonic belt (SBPB) showing the eastward younging of the plutons (after Farris and Paterson 2009). Numbers other than ages are $\varepsilon(\mathrm{Hf})_t$ values of plutons of the SBPB from Roig (2014) and Arntson et al. (2017) and recalculated values from Barker et al. (1992) and Sisson et al. (2003); see table S5. AT = Aleutian Trench; CT = Chugach terrane; PWT = Prince William terrane; WCT = Wrangellia composite terrane; YT = Yakutat terrane. CIP = Crawfish Inlet pluton; EHP = Eagle Harbor pluton; MDP = Mount Draper pluton; MKP = McKinley pluton; NOG = Novatak glacier pluton; NGP = Nunatak glacier pluton; RRP = Rude River pluton; SBP = Sheep Bay pluton; SP = Mt. Stamy pluton; VCGP = Van Cleve glacier pluton. A color version of this figure is available online.

area of the St. Elias syntaxis at the Yakutat plate corner, where transform motion along Fairweather fault changes to flat-slab subduction (Enkelmann et al. 2009, 2010, 2015; Falkowski et al. 2014; Falkowski and Enkelmann 2016; Dunn et al. 2017). Imbricated Eocene to Holocene sediments of the preorogenic Kulthieth (middle Eocene) and Poul Creek (lower Oligocene to lower Miocene) Formations and the synorogenic Yakataga (Miocene through Holocene) Formation form a fold-and-thrust belt up to 15 km thick overlying the western part of the Yakutat terrane (Plafker 1987; Plafker et al. 1994; Worthington et al. 2010; Enkelmann et al. 2015). The eastern part consists of the Yakutat Group, part of the Chugach flysch and mélange (Plafker 1987; Plafker et al. 1994).

To the northeast follow the Jurassic to Tertiary plutonic (ca. 45–190 Ma) and associated metamorphic rocks of the Coast Plutonic Complex (CPC) that extend from Washington State to southwest Yukon (fig. 1*A*; Gehrels et al. 2009; Mahoney et al. 2009). They separate the Wrangellia terrane from the Stikine terrane in the east.

The Surveyor Fan System. The Surveyor Fan can be divided into two depositional sequences based on seismic data (Stevenson and Embley 1987). The older sequence represents turbiditic deposition since ca. 9.7 Ma, in the Miocene (Stevenson and Embley 1987; Rea and Snoeckx 1995). In view of the absence of a major channel system, it is undecided whether sediment transport in the older sequences of the fan occurred without development of a main channel system or whether a channel system was originally present in the north and has already been subducted into the Aleutian Trench (Stevenson and Embley 1987). Since the beginning of deposition, northwestward movement of the Pacific plate, including a component of that motion of the Yakutat terrane, has been accommodated by dextral transform movement along the North American plate margin (Stevenson and Embley 1987; Plafker et al. 1994; Reece et al. 2011). This consequently led to potentially significant changes in the provenance of the deposits with time.

Deposition of the younger sequence has lasted from ca. 5 Ma to the present (Hogan et al. 1978; Reece et al. 2011; Gulick et al. 2015). A noteworthy characteristic of the Surveyor Channel is that it is not linked to a major fluvial system (Ness and Kulm 1973; Carlson et al. 1996; Reece et al. 2011). Today, glaciers are the main sediment suppliers, and sediment routing into the ocean is accomplished through several shelf-crossing gullies that merge to form three main channels that join ca. 150 km from the continental margin to form the Surveyor Channel (the Icy, Yakutat, and Alsek legs; fig. 1*A*). The Surveyor Channel has been the main sediment-routing system since at least ca. 2.7 Ma (Gulick et al. 2015). The Alsek leg might have existed since the Miocene-Pliocene boundary and the onset of glaciation at that time (Reece et al. 2011). The Bering, Malaspina, and Hubbard glaciers (fig. 1*B*) form the biggest glaciers in the Gulf of Alaska region today (Molnia 2008). The Bagley icefield and the adjacent Bering glacier drain the orogen to the southwest. Ice flow of the Seward-Malaspina glacial system, draining to the southeast, is separated from the Bering glacier (Bruhn et al. 2012). The Seward glacier is funneled through the Seward Throat before flowing into the Malaspina piedmont glacier (Bruhn et al. 2012; Headley et al. 2013), delivering material into the Yakutat and Alsek legs, the two main tributaries of the Surveyor channel. The Hubbard glacier and the Alsek glacial system also feed material into these tributaries (Reece et al. 2011). The Yakutat leg experienced ca. 35 km of lateral relocation to the southeast because of its proximity to a basement high and an overlying sediment wedge that grew to the southeast (Reece et al. 2011). The other legs did not experience lateral movement (Reece et al. 2011). The Icy leg connected to now partially buried sea valleys and had received input from the Bering glacier before it was shut off after the onset of glacial interval C (fig. 3; Reece 2011). The Surveyor Channel discharges into the Aleutian Trench ca. 700 km from the continental margin (Stevenson and Embley 1987; Carlson et al. 1996; Dobson et al. 1998; Reece et al. 2011).

Sedimentation rates on the distal fan started at ~30–70 m/My between 5.2 and 2.8 Ma and doubled to peak values of 120 ± 20 m/My between 2.4 and 2.0 Ma in response to the expansion of Northern Hemisphere glaciation at the Plio-Pleistocene boundary (Gulick et al. 2015). In distal locations of the Surveyor Fan, ca. 460 km southwest of the present shoreline, the first glacial diamicts appear at ca. 2.6 Ma, after the mid-Pliocene warm interval (Rea and Snoeckx 1995; Jaeger et al. 2014). Reduced sedimentation rates of ~60 m/My from 1.6 to 1.2 Ma indicate an apparent reduction of regional glacial erosion (Gulick et al. 2015). Coinciding with the MPT, sedimentation rates rose to peaks of ~140 m/My by 0.8 Ma and even higher at more proximal sites (80 cm/ka at site U1418, 130 cm/ka on the shelf, and up to 300 cm/ka on the slope; Gulick et al. 2015). Since ca. 2.5 Ma, glaciers have reached the edge of the continental shelf several times during glacial maxima; the glacial extent during the Last Glacial Maximum has been mapped in figure 1*B* (Mann and Hamilton 1995; Berger et al. 2008*a*).

Sampling

Sampling was performed on fine sand and silt intervals from sites U1417 and U1418 drilled during IODP Expedition 341 in the distal and proximal Surveyor Fan, respectively (Expedition 341 Scientists 2014). Depths are reported in meters as core composite depth below seafloor (m CCSF-B; Jaeger et al. 2014).

Site U1417 is situated in the distal Surveyor Fan ca. 60 km west of today's Surveyor Channel (fig. 1*A*), receiving input from the Alsek, Yakutat, and Icy legs (Expedition 341 Scientists 2014; Dunn et al. 2017). It recovered Miocene (ca. 10 Ma) to Holocene sediments from a maximum depth of ca. 700 m (CCSF-B; fig. 3). Lithostratigraphic units I–V are in line with hemipelagic/pelagic rainout and overbank levee deposition from turbidity currents (Expedition 341 Scientists 2014; fig. 3).

Site U1418 is situated between an active channel and an abandoned channel-like structure (Bering Channel), both with an Aleutian Trench terminus, originating seaward of the continental shelf break between the Bering Trough and the Pamplona Zone (fig. 1*A*; Expedition 341 Scientists 2014). It recovered early Pleistocene to Holocene sediments from a maximum depth of ca. 950 m. The lowermost lithostratigraphic unit is interpreted as a mass transport deposit (MTD) recording early Pleistocene massive slope failure (unit IV; fig. 3; Reece et al. 2011; Expedition 341 scientists 2014). The upper units are inferred to have formed through hemipelagic settling and gravity flows from the neighboring channels (Reece et al. 2011; Expedition 341 Scientists 2014). Units II and I are

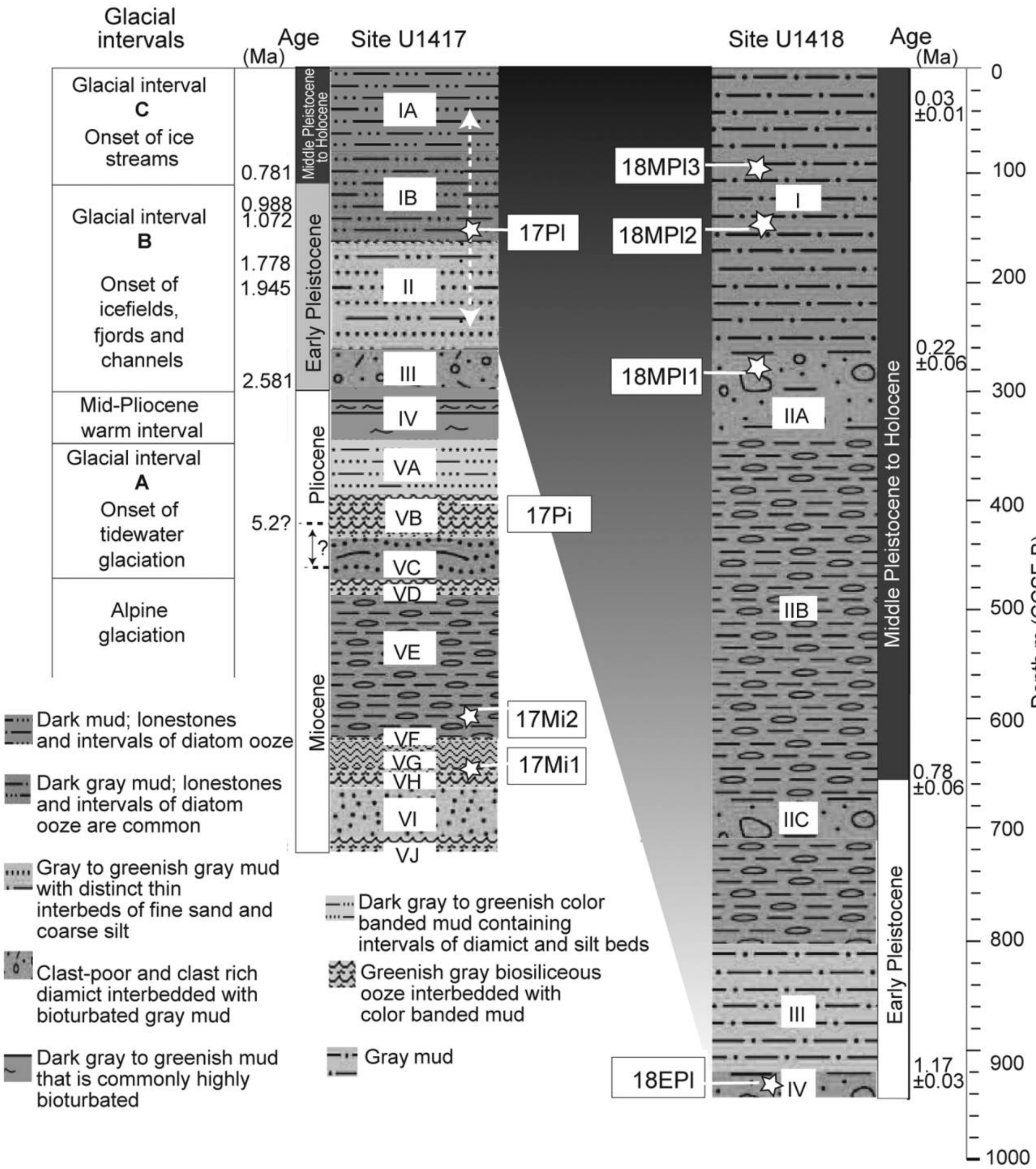

Figure 3. Lithostratigraphy of Integrated Ocean Drilling Program Expedition 341 sites U1417 (distal site) and U1418 (proximal site) and climatic events in southern Alaska. Sample positions are marked with white stars. Modified after Lagoe et al. (1993) and Expedition 341 Scientists (2014). A color version of this figure is available online.

considered to correlate with units II and I at the distal site (fig. 3; Expedition 341 Scientist 2014). Sediments are unconsolidated and consist mostly of muddy and silty material, with some contribution of fine sand and thick intervals of diamict.

We sampled four intervals at each site, covering material from the Miocene (turbidite sequence), the Miocene-Pliocene boundary (beginning of Surveyor Channel transport and intensification of glaciation), and the early and middle Pleistocene (intensification of glaciation at the MPT; fig. 3). Sample names start with the abbreviated name of the site from which they were chosen (17 and 18 for U1417 and U1418, respectively), followed by the abbreviated name of the stratigraphic interval (Mi for Miocene, Pi for Pliocene, EPe for early Pleistocene, MPe for middle Pleistocene, and Pe for Pleistocene). If more than one sample was processed for one interval, a number is attached, starting with 1 for the stratigraphically oldest sample. Some samples are composite samples (see the appendix, available online). Time of deposition was deduced from bio- and magnetostratigraphic reconstructions (Jaeger et al. 2014; Gulick et al. 2015).

Methods

Samples were wet-sieved to remove mud. Zircons were selected from the size fractions 0.063–0.25 mm by density separation and magnetic sorting with a Frantz magnetic separator followed by handpicking under a binocular microscope.

U-Pb Dating. Grains were randomly handpicked and mounted on 1-inch epoxy mounts. For most samples, all zircons available in each fraction were picked to get the highest possible number of zircon grains out of the limited sample volume. No selection was made regarding grain size, shape, or color. The grains were embedded into epoxy pucks and polished for cathodoluminescence (CL) analysis performed with a JEOL 6610 scanning electron microprobe. All mounted grains were dated to minimize operator influence. The grains were analyzed by laser ablation (LA) ICP-MS at the Institute for Mineralogy at the University of Münster. Laser spots were set in the cores and rims of the grains if possible (two spots per grain) with a diameter of 25 or 35 μm, depending on the size of the zircon zonations. Some grains were too small to measure core and rim (for details of analytical methods, see the appendix). Age data were processed for visualization with DensityPlotter (Vermeesch 2012), showing normalized kernel density estimation. The bandwidth of the kernel density estimations was calculated by an algorithm implemented in the program on the basis of the diffusion equation (Botev et al. 2010; Vermeesch 2012).

Hf Isotopes. Analyses of Lu-Hf isotope systems were carried out by LA-ICP-MS at Goethe University, Frankfurt. A subset of grains representing all U-Pb age groups was selected for measuring (for analytical details, see the appendix). Round Lu-Hf spots of 43 μm were placed on top of or next to the previously measured U-Pb age spots. Hf isotope data of zircon are usually reported in the epsilon notation $\varepsilon(\mathrm{Hf})_t$, where the measured $^{176}\mathrm{Hf}/^{177}\mathrm{Hf}$ is normalized to the $^{176}\mathrm{Hf}/^{177}\mathrm{Hf}$ of the undifferentiated mantle (chondritic uniform reservoir [CHUR]), with positive $\varepsilon(\mathrm{Hf})_t$ values representing input from a mantle source that experienced earlier depletion while negative $\varepsilon(\mathrm{Hf})_t$ values suggest incorporation of a preexisting crustal component into the evolving magma (Siebel and van den Haute 2009). The $\varepsilon(\mathrm{Hf})_t$ values were calculated with the apparent U-Pb age determined by LA-ICP-MS dating.

Rare Earth Elements. Rare earth elements (REEs) were measured for selected grains that were previously dated by U-Pb. Measurement was performed by LA-ICP-MS at the Institute for Mineralogy at the University of Münster. Laser spots with a diameter of 35 μm were set in the cores of the grains, avoiding impurities and cracks (for analytical details, see the appendix).

(U-Th)/He Dating. (U-Th)/He dating was applied to Miocene to Pliocene samples from site U1417. From samples 17Mi1–17Mi2 and 17Pi, 70 zircons (37 and 33, respectively) were selected for (U-Th)/He analysis performed at the GÖochron Laboratories of the Geozentrum, University of Göttingen (for analytical details, see the appendix). Component identification was performed with two methods, using PopShare (Dunkl and Székely 2002) and DensityPlotter (Vermeesch 2012) software.

Results

The sample volume was restricted because of the limited amount of material present in the drill core half supplied for sampling (6.2 cm in diameter) and the small grain size of the samples (mostly muddy to silty, with local fine sand layers). Zircon yield was very small and for some samples was nearly zero. All Pleistocene sediments at site U1417 were very muddy, and heavy-mineral content was low. These samples supplied very few to no zircons.

All zircons are euhedral to subrounded, 70–250 μm in length, and all have a short-prismatic to long-prismatic shape. Color ranges from colorless to slightly pinkish. The CL pictures show a large variety of zonations (fig. 4): oscillatory-growth zoning, banded zoning, complex patchy cores, linear-growth zoning, and sector zoning. Many grains have a pitted surface, with cavities truncating the core. Some show dark or bright rims. Some grains did not allow analysis of a core and a rim spot for U-Pb dating because of small grain size. Inclusions, high common-lead contents, or a short analytical signal represented obstacles to meaningful age determination.

U-Pb Dating. A total of 1127 U-Pb ages from 651 zircon grains were measured (fig. 5; table S1; tables S1–S5 are available online). U-Pb ages of zircon

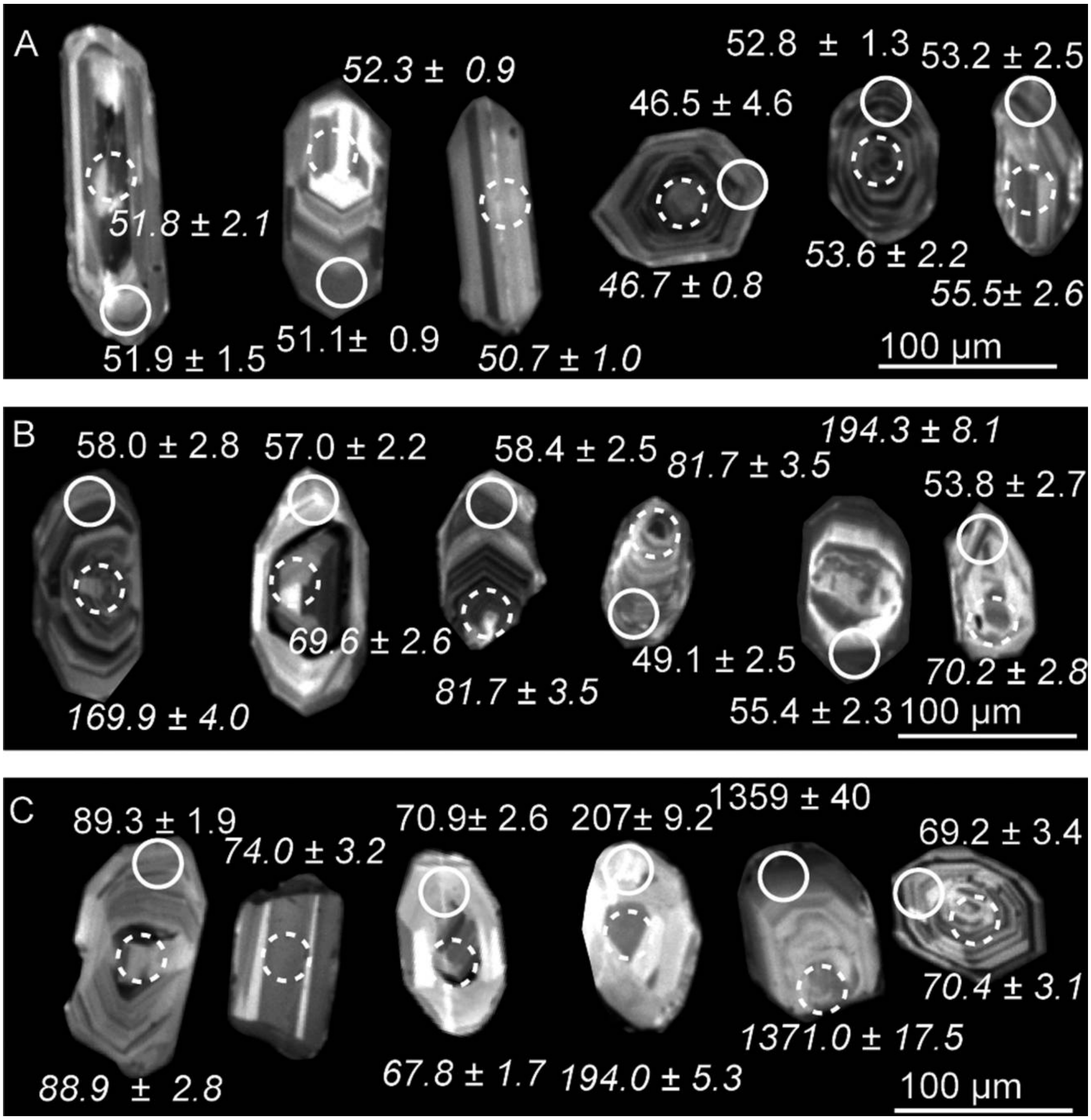

Figure 4. Representative cathodoluminescence images of zircons from site U1417 and U1418 sediments and associated U-Pb ages. Dashed circles mark the positions of core analyses; solid circles mark the positions of rim analyses. Rim ages are in italics. *A*, Zircons showing overlapping core and rim ages of ca. 50–60 Ma (group 1); *B*, grains with a rim of ca. 50–60 Ma and an inherited (xenocrystic) older core (group 2); *C*, zircons showing overlapping core and rim ages of >63 Ma (group 3).

record the crystallization time or resetting during a high-temperature metamorphic event (Cherniak and Watson 2001; Rahl et al. 2003). Combining U-Pb dating and CL imaging gives information on crystallization ages of different domains of each crystal, revealing detailed information on its growth history (Koschek 1993). The southern Alaska margin comprises a mixed magmatic and metasedimentary source area (Plafker 1987; Plafker et al. 1994). Especially with metamorphic peak conditions in the CMC allowing formation of metamorphic zircon rims that overlap in age the emplacement of intrusions of the SBPB (e.g., Gasser et al. 2012), detailed analyses of zircon CL images and dating of cores as well as rims

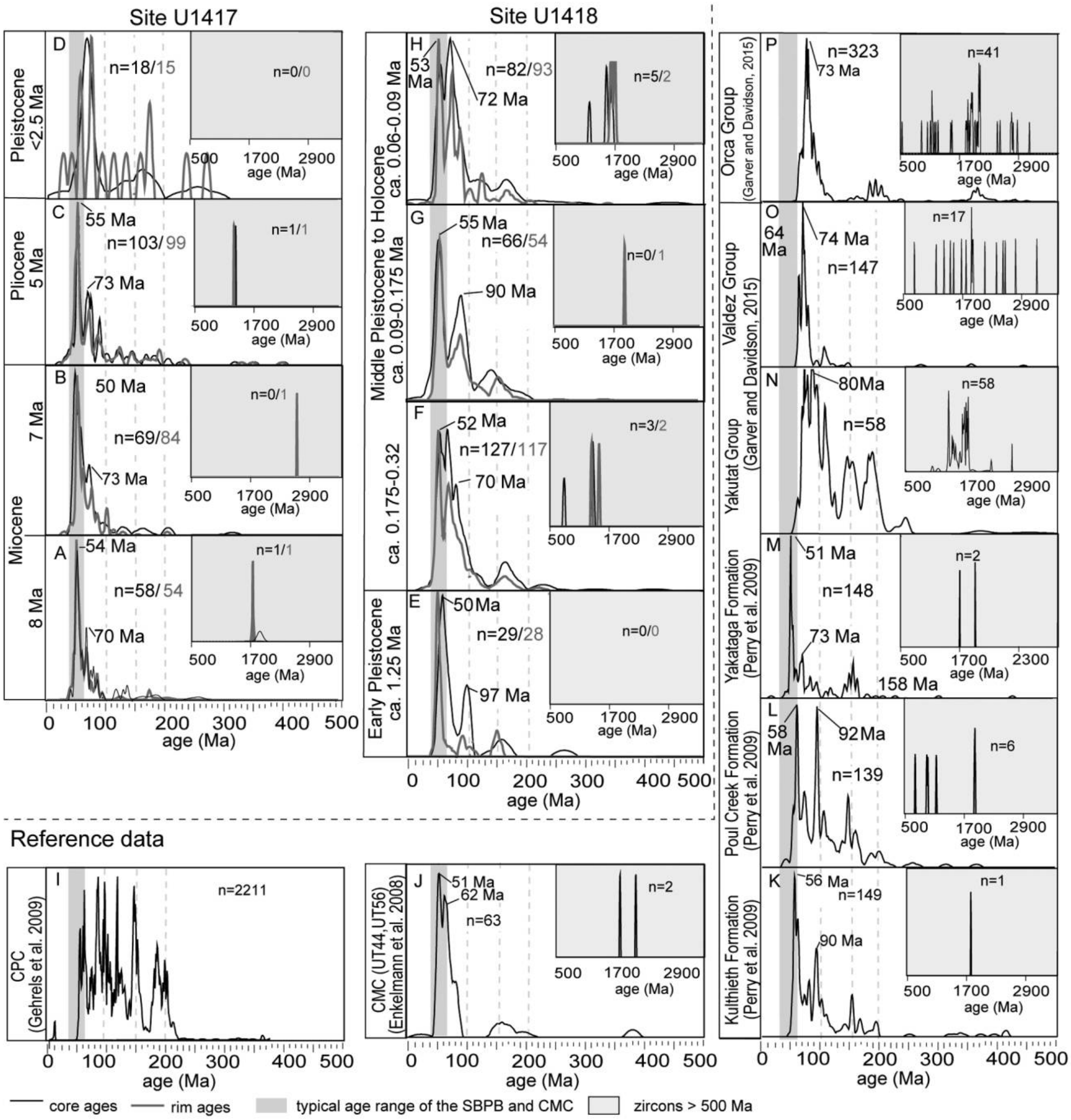

Figure 5. Normalized kernel density estimate distributions of U-Pb laser ablation ICP-MS ages of zircon cores and rims of sediments from Integrated Ocean Drilling Program sites U1417 (distal site; *A–D*) and U1418 (proximal site; *E–H*; this study) and of zircon core U-Pb ages from the Valdez, Orca, and Yakutat Groups; the Kulthieth, Poul Creek, and Yakataga Formations; the Coast Plutonic Complex (CPC) and the Chugach Metamorphic Complex (CMC; *I–P*; from Enkelmann et al. 2008; Gehrels et al. 2009; Perry et al. 2009; Garver and Davidson 2015). Sample names are 17Mi1 (*A*), 17Mi2 (*B*); 17Pi (*C*); 17Pl (*D*); 18EPl (*E*), 18MPl1 (*F*); 18MPl2 (*G*), and 18MPl3 (*H*). SBPB = Sanak-Baranof plutonic belt. A color version of this figure is available online.

are crucial to discriminate the different source rocks (Moecher and Samson 2006).

All samples show Paleogene to Precambrian ages (fig. 5; table 1). Only sample 18EPl shows a limited age range, with an oldest detrital zircon age at 264 ± 4 Ma. The majority of grains in all samples are younger than ca. 340 Ma. All samples have a main age component of ca. 50–55 Ma. Most samples have a second age component at ca. 70 Ma; only samples 18EPl and 18MPl2 show second age components of 97 and

Table 1. Numbers of Zircon Grains from Sites U1417 and U1418 Dated by U-Pb, with U-Pb Age Ranges and Time of Deposition for Each Sample

Sample	Sample depth (m CCSF-B)	Sedimentation age (Ma)	n	U-Pb ages (Ma) Minimum	U-Pb ages (Ma) Maximum	Most ages (Ma)	Main age components 1	Main age components 2	Double-dated grains	Grains with inherited cores
U1417:										
17Pl	40–243	<2.5	23[a]	32 ± 5	281 ± 10	. . .	. . .	. . .	12	1
17Pi	400–438	4–5	118	24 ± 1	1317 ± 22		55	73	86	5
17Mi2	604	7.4–8	86	28 ± 2	2666 ± 26	<318	50	73	68	10
17Mi1	632–642	10–13	65	39 ± 2	1907 ± 43	<270	54	70	49	12
U1418:										
18MPl3	97–119	.06–.09	112	2.5 ± .5	1788 ± 32	<332	53	72	82	11
18MPl2	140–170	.09–.175	73	35 ± 2	1730 ± 5	<340	55	90	48	7
18MPl1	280	.3–.175	143	32 ± 2	1475 ± 64	<250	52	70	106	21
18EPl	939	1–1.5	143	44 ± 2	264 ± 4	<264	50	97	23	6

Note. CCSF-B = core composite depth below seafloor.
[a] We prepared 14 Pleistocene samples; only three provided some zircons that are summarized in this sample. Therefore, we have only 19 grains dated from Pleistocene unit 1 and 4 from unit 2.

90 Ma, respectively. All samples show grains with inherited cores and younger rims. Most rim ages are ca. 40–50 Ma, while core ages range from ca. 62 to 1244 Ma. Details of analyzed grains, the youngest and oldest grains per sample, age components, and the number of grains with inheritance are given in tables 1 and S1. On the basis of the U-Pb age spectra (fig. 5) and the comparison of core and rim ages of each zircon, we identify three main groups of zircons present in all samples. These are (1) zircons of ca. 50–60 Ma with overlapping core and rim ages (fig. 4*A*), (2) xenocrystic zircons with rims of ca. 50–60 Ma and inherited older cores ranging from 62 to 1244 Ma (fig. 4*B*), and (3) zircons of >63 Ma that lack a metamorphic rim (fig. 4*C*).

To account for the information stored in the core and rim data, we evaluate the number of grains that can be assigned to groups 1–3 (fig. 9). We give a range for the number of grains that belong to each group. Here, the minimum number represents the number of grains that can be assigned to a specific group unambiguously. The maximum number includes the zircons that could also belong to another group because of the lack of a core or rim age data. The sediments from site U1417 show a decrease in groups 1 (21%–38%) and 2 (4%–15%) and an increase in group 3 (29%–58%) zircons from the Miocene to the Pleistocene. Only the number of group 2 zircons in the Pleistocene sample diverges from this pattern, being similar to that of the Pliocene sample. Still, the range of the number of group 2 zircons is large, especially for the Pleistocene sample, lowering its significance.

The samples from site U1418 all show relatively high numbers of group 3 zircons (46%–62%). The number of group 2 zircons slightly increases with younger depositional age (8%–12%), even though the range between the minimum and maximum number of grains belonging to each group somewhat limits the discriminative power of the data. Group 1 zircons contribute 19%–34% to the sediments, not showing a continuous trend. Only sample 18EPl diverges from this pattern, showing higher numbers of group 1 (38%) and 2 (31%) zircons and lower numbers of group 3 zircons.

Statistics. We compared the Surveyor Fan zircon age spectra to literature data (reference materials) from the Yakataga, Kulthieth, and Poul Creek Formations and the Yakutat, Orca, and Valdez Groups (fig. 5*I*–5*N*), a representative sample from the CPC, and two plutons of the SBPB for which we could find a large set of U-Pb ages (Sheep Bay and McKinley plutons), using a multidimensional scaling (MDS) analysis plot generated with the "provenance" algorithm (fig. 10; Vermeesch et al. 2016). All middle Pleistocene samples from site U1418 and the Pliocene sample from site U1417 form a dense cloud with the Yakataga Formation, supporting similar sources. Furthermore, they plot in the middle of all reference samples, indicating that they are a mixture of all. The Miocene samples from site U1417 plot closer to the pluton samples, indicating that they record higher input from the SBPB. Only the Pleistocene sample from site U1417 plots close to the CPC and the Poul Creek Formation, but the low grain number lowers the significance.

Hf Isotope Systematics. Our data set provides 468 age-corrected $\varepsilon(\mathrm{Hf})_t$ values for zircons from the Surveyor Fan dated by U-Pb (fig. 6; table S2). All samples have grains with the same $\varepsilon(\mathrm{Hf})_t$ characteristics. Most grains younger 70 Ma give $\varepsilon(\mathrm{Hf})_t$ values of −5 to +5, with some grains having values within the range

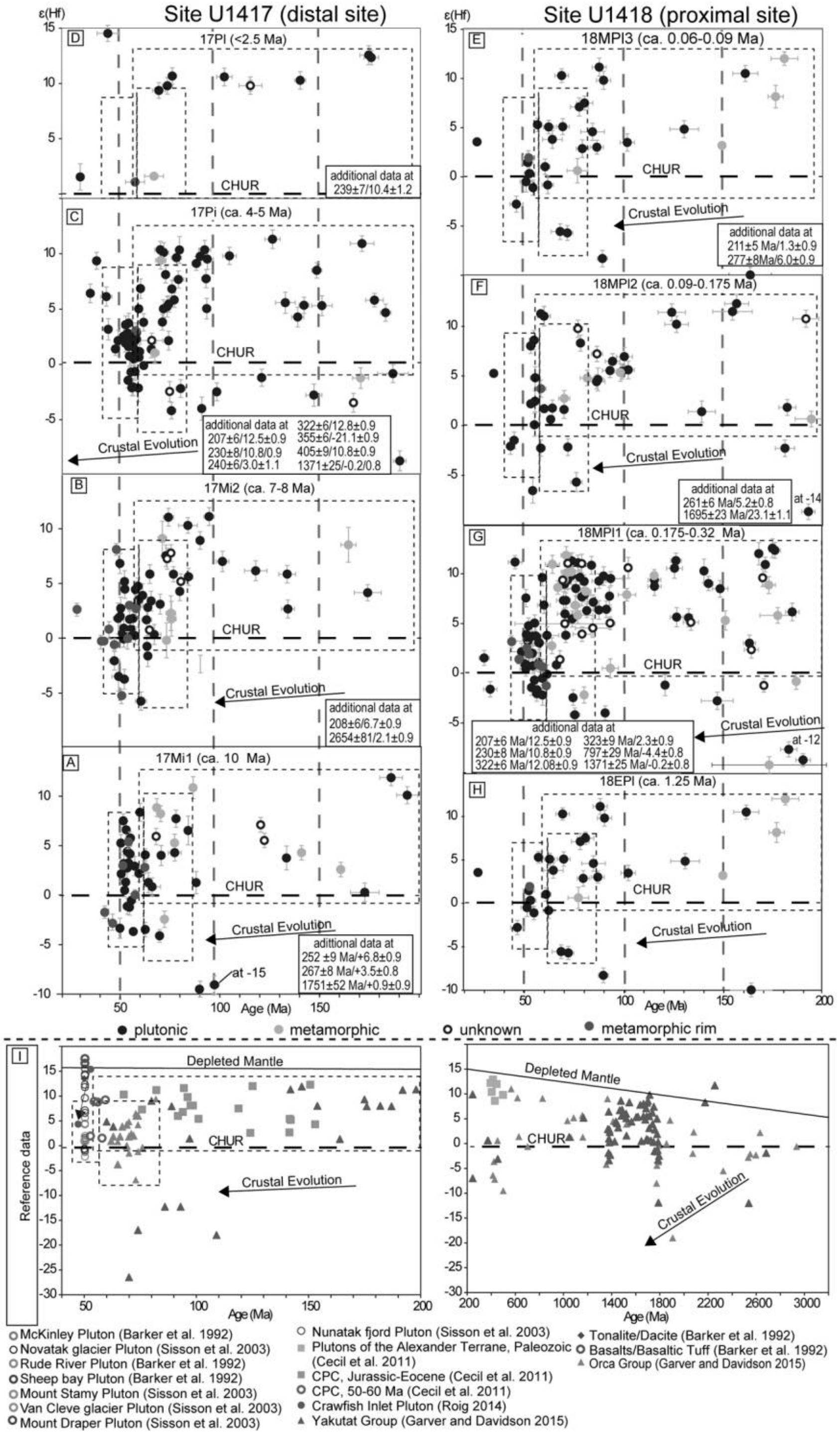

Figure 6. Laser ablation ICP-MS $\varepsilon(\mathrm{Hf})_t$ values for zircons from sites U1417 and U1418 (*A*–*H*; this study) and onshore reference samples (*I*; Barker et al. 1992; Sisson et al. 2003; Perry et al. 2009; Cecil et al. 2011; Roig 2014; Garver and Davidson 2015). Sample names are 17Mi1 (*A*); 17Mi2 (*B*), 17Pi (*C*), 17Pl (*D*), 18EPl (*E*), 18MPl1 (*F*), 18MPl2 (*G*), and 18MPl3 (*H*). CHUR = chondritic uniform reservoir. A color version of this figure is available online.

of −7 to +15. Zircons with ages of >70 Ma have $\varepsilon(\mathrm{Hf})_t$ values that vary from −23 to +13, with most grains between +4 and +13. The Precambrian grains show $\varepsilon(\mathrm{Hf})_t$ values of −0.4 to +4.5, which would provide as a source for 70 Ma granites a calculated $\varepsilon(\mathrm{Hf})_t$ of −37 to −28.

REEs. Ninety-four REE spectra were measured for the whole age range present in samples 17Mi, 17Pi, and 18MPl1–18MPl3 (table S3). Most grains show moderate to pronounced negative Eu and positive Ce anomalies (fig. 7). Some show very low Ce and low to medium Eu anomalies. Grain age and the scale of Ce and Eu anomalies do not correlate and are also independent of deposition age.

(U-Th)/He Dating. The 37 (U-Th)/He ages measured for samples 17Mi1 and 17Mi2 range from 6.9 ± 0.7 to 114.1 ± 10 Ma (table S4; fig. 8). Sample 17Pi provided 40 ages from 12.4 ± 0.8 to 136.3 ± 12 Ma. The cumulative plot (fig. 8) shows that the majority of the zircons in both samples are Eocene and younger in age. Both methods applied for component identification yielded essentially similar results. In both samples there are three age components, namely, Late Cretaceous (rather diffuse), Eocene, and late Oligocene (table 2). Their mean values are similar to identical. The (U-Th)/He zircon (ZHe) ages in sample 17Pi have a wider spread than those in samples 17Mi1 and 17Mi2. The sample also contains a Miocene age component and some weak indications of the presence of Early Cretaceous ages.

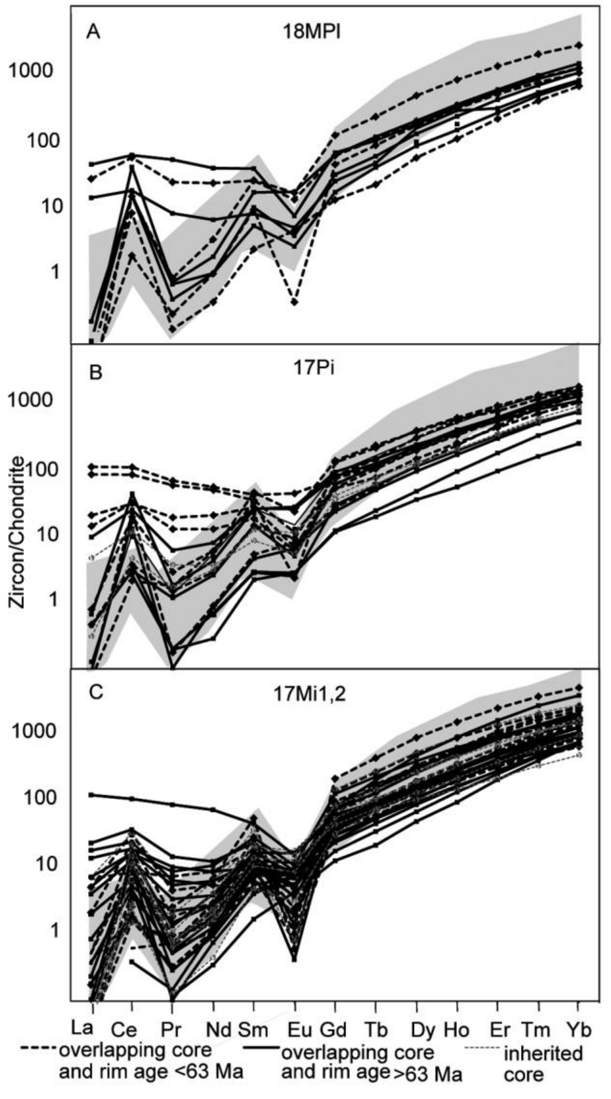

Figure 7. Chondrite-normalized rare earth element (REE) patterns of representative zircons from sites U1417 and U1418. Shaded area shows range of REE spectra from zircons of a metaigneous gneiss from the Chugach Metamorphic Complex (Gasser et al. 2012).

Derivation of the Sediments

The composition of sediment generated by weathering and erosion strongly depends on the respective mineral fertilities of the involved source-rock types. Caution is therefore advised when drawing conclusions on quantitative input from available source rocks. Considering zircon age distributions, lithologies with low zircon fertilities result in these source rocks and areas being underrepresented in zircon populations (Moecher and Samson 2006; O'Sullivan et al. 2016). At the southern Alaska continental margin, a great variety of rock types crop out (e.g., Plafker et al. 1994). Twenty-four of 79 cobbles of fine-grained metasediments and mafic rocks around the Malaspina glacier have already been found to lack any zircon (Grabowski et al. 2013), supporting that zircon fertility markedly influences quantitative provenance information. To account for the information lost through variable zircon fertilities, additional single-grain geochemical analyses of other heavy minerals have been performed (Huber et al. 2018). Still, intersample comparison of the abundances of zircon from different source areas supplies insight into changing input from all zircon-bearing source rocks. A higher concentration of material from one source relative to other sources can always be caused by an increase of input from this source as well as a decrease of input from the other sources. Therefore, the zircon abundances can be interpreted only as relative changes.

U-Pb Age Provenance of Detrital Zircons. We can assign each of the three groups of zircons identified to certain source areas in southern Alaska. Group 1 has a ca. 50–60 Ma age maximum and overlapping core and rim ages (fig. 4*A*). Potential source rocks are the ca. 50–60 Ma intrusions of the SBPB and the CPC (figs. 1, 2). The zircon age range of the SBPB varies from ca. 60 Ma in the west to ca. 50 Ma in the east (fig. 2; Bradley et al. 1993, 2003; Farris et al. 2006; Gasser et al. 2012). In the Yakutat segment of the belt, between Prince William Sound and the Nunatak Fjord, main crystallization ages are 55–52 Ma

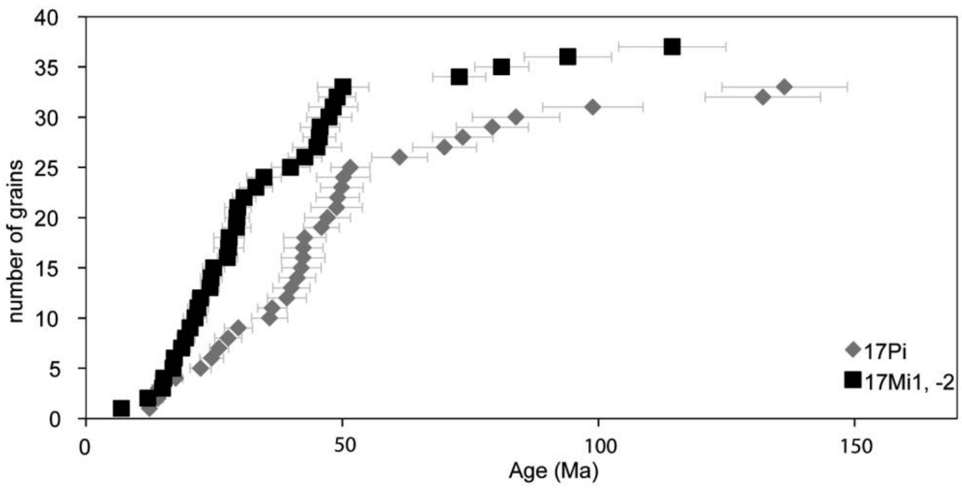

Figure 8. (U-Th)/He age distribution of zircons from samples 17Mi1–17Mi2 and 17Pi.

(fig. 2; Gasser et al. 2012), matching one of the main age components found in the samples (fig. 5*A*–5*H*).

The CPC crops out farther to the east (fig. 1*A*). The igneous rocks in that area are mostly tonalitic and show ages of 50–160 Ma (Gehrels et al. 2009). Especially for the late Miocene sediments, it is a realistic source, considering the northwest-directed movement of the Yakutat and Pacific plates (fig. 1*A*). The CPC has been inferred to have abundantly contributed material to the sediments of the Poul Creek and Kulthieth Formations on the Yakutat terrane (Perry et al. 2009), but input from the CPC decreases strongly in the Yakataga Formation (Perry et al. 2009), which was deposited at the same time as the Surveyor Fan sediments. Westward transport by the Alaska Current and/or reworking of the Poul Creek and Kulthieth Formations might still have fed some material from the CPC into the fan deposits. Comparison of the amount of 50–60 Ma zircons in the sediments from sites U1417 and U1418 with their abundances in the Poul Creek and Kulthieth Formations, however, supports strong input from an additional source that provides a large number of ca. 50–60 Ma zircons (fig. 5*J*, 5*I*). Therefore, we favor the plutons of the SBPB as the main source for most of these zircons, but direct or indirect (reworking of sediments) contribution of material from the CPC is possible.

Group 2 has rims of ca. 50–60 Ma and inherited xenocrystic older cores ranging from ca. 62 to 1244 Ma. At ca. 750°C (Bruand et al. 2014), the highest metamorphic temperatures in the potential source area were reached within the CMC. This was not high enough to reset zircon U-Pb ages (Bruand et al. 2014). Still, zircons from this complex show metamorphic rims and inherited cores; the rims very likely formed during partial melting at the metamorphic peak (Gasser et al. 2011). Zircon rim ages in the CMC were found to be 53–54 Ma; inherited core ages range between 61 and 247 Ma (Gasser et al. 2012). Core and rim ages found for the xenocrystic zircons from sites U1417 and U1418 match ages that support that these zircons are sourced from the metamorphic rocks of the CMC. Another source for this kind of zircon are the plutons of the SBPB. A small number of inherited cores have been found within zircons from the Hive Island pluton (Davidson and Garver 2017). There is

Table 2. Age Components Identified by Simplex Algorithm (Dunkl and Székely 2002) in the Zircon (U-Th)/He Single-Crystal Ages Obtained from Samples 17Pi and 17Mi1–17Mi2

	17Pi		17Mi1–17Mi2	
Component	Mean ± SD (Ma)	Approximate proportion (%)	Mean ± SD (Ma)	Approximate proportion (%)
Miocene	14 ± 2	12		
Late Oligocene	25 ± 3	13	24 ± 8	70
Eocene	44 ± 6	55	47 ± 3	21
Late Cretaceous	77 ± 8	14	86 ± 13	9
Early Cretaceous	~132 ± 2[a]	6		

[a] Only indication, represented by two data.

no information on other plutons of the SBPB with inherited zircons, indicating that inherited zircons make up only a minor part of their zircon yield. Some zircons with ca. 50–60 Ma rims and inherited older cores have been reported from the CPC at the latitude of the southern end of Queen Charlotte Island, while zircons from farther north in the complex have thus far not been found to be characterized by inheritance (Gehrels et al. 2009; Cecil et al. 2011). Therefore, some of the zircons might have a CPC origin, but a CMC origin appears more likely.

Group 3, zircons older than 63 Ma, have no discernible metamorphic rim (fig. 4*C*). The age distributions older than 63 Ma of sites U1417 and U1418 are similar to the age spectra of the low-grade metamorphic areas of the flysch of the Orca and Valdez Groups in the fold-and-thrust belt; the Kulthieth, Poul Creek, and Yakataga Formations; and the rocks of the Yakutat Group south and west of the CMC (fig. 5). These (meta-)sediments store the entire age spectrum of their ancestral source rocks. The Orca, Valdez, and Yakutat Groups are dominated by Jurassic–Cretaceous grains derived from magmatic-arc rocks in the CPC (Garver and Davidson 2015). In addition, these rock units contain up to 10% Precambrian grains (Garver and Davidson 2015). Single Precambrian grains are also present in our Surveyor Fan samples.

Another source might be the CPC, providing grains of mostly Jurassic through Tertiary age, or the Wrangellia composite terrane that feeds mostly zircons of Early Cretaceous and older age (e.g., Dodds and Campbell 1988; Plafker et al. 1994; O'Sullivan and Currie 1996; Enkelmann et al. 2010; Garver and Davidson 2015). Plutonic activity between 110 and 90 Ma and between 70 and 80 Ma in the CPC (Armstrong 1988) matches important age peaks of the sediments from sites U1417 and U1418. With the Orca, Valdez, and Yakutat Groups having been most likely fed by the CPC (Garver and Davidson 2015), direct input from the CPC and reworking of these coast-proximal sources can provide similar age spectra. Still, the low congruence with the CPC reference samples (figs. 5*A*–5*E*, 10) suggests that the CPC was a minor source at best.

The Wrangellia composite terrane comprises rocks that are mostly Early Cretaceous/Jurassic in age and older, together with some younger material of the Wrangell plutonic suite and lava (mid- to late Miocene; Plafker 1987; Dodds and Campbell 1988). Upper Jurassic plutonic rocks are widespread in the St. Elias Mountains north of the Border Ranges fault, extending into today's Seward-Malaspina and Hubbard glacier catchments (Armstrong 1988; Dodds and Campbell 1988; Falkowski et al. 2016). With most of the zircons of group 3 being ca. 60–100 Ma in age, the Wrangellia composite terrane seems to have been a minor source at best.

Provenance Affiliations Indicated by Hf Isotopes. We use the Hf isotopes of the zircons dated by the U-Pb method to further constrain their provenance. The Hf isotope systematics of zircons gives information on the crustal evolution of their source rock (Amelin et al. 2000; Kinny and Maas 2003). Because of the scarcity of published Hf isotope data from the source area, we also use $\varepsilon(\mathrm{Hf})_t$ values recalculated from $\varepsilon(\mathrm{Nd})$ values with the equation for the crustal array of Vervoort et al. (1999; fig. 2; table S5).

Most of the zircons of group 1 (plutonic source; SBPB or CPC provenance) have $\varepsilon(\mathrm{Hf})_t$ values of -5 to $+5$ (fig. 6*A*–6*H*), similar to those of the intrusions of the SBPB cropping out from Baranof Island to Cordova (fig. 2), supporting the source affiliations indicated by U-Pb dating. The plutons of the SBPB formed as near-trench forearc plutons connected to subduction of a spreading ridge and have a mixed source of melted greywacke and argillite from the accretionary prism (up to 65%–90%) and variable amounts of more mafic mantle-derived components, such as mid-ocean ridge basalt, causing varying $\varepsilon(\mathrm{Hf})_t$ values throughout the belt (Moore et al. 1983; Barker et al. 1992; Bradley et al. 1993, 2003; Harris et al. 1996; Cowan 2003; Haeussler et al. 2003; Sisson et al. 2003; Farris et al. 2006; Madsen et al. 2006; Farris and Paterson 2009; Arntson et al. 2017). Melts in the western part of the belt assimilated larger amounts of sedimentary country rock than those in the eastern part, which experienced higher amounts of mantle input (Farris and Paterson 2009). Locally, the contribution of the two sources varies from pluton to pluton and even within individual plutons, where $\varepsilon(\mathrm{Hf})_t$ values can vary because of a variable mantle contribution during emplacement (see Crawfish Inlet pluton; figs. 2, 5*I*; Farris and Paterson 2009; Roig 2014). This inhibits association of certain $\varepsilon(\mathrm{Hf})_t$ values with different sections of the SBPB. The 50–60 Ma zircons from the CPC show $\varepsilon(\mathrm{Hf})_t$ values of ca. $+9$ to $+10$ and $+1$ to $+2$ (Cecil et al. 2011), also overlapping the values found within the group 1 zircons, but do not provide the complete range observed. At present, the CPC cannot be ruled out as source for zircons of group 1 but is less likely than the SBPB.

Most $\varepsilon(\mathrm{Hf})_t$ values of zircons from group 2 (metamorphic rim) range between ca. -5 and $+7$, matching the values found to be typical for the SBPB (fig. 6). The inherited cores give a wide range of $\varepsilon(\mathrm{Hf})_t$ values, -10 to $+15$, similar to values for the Orca and Yakutat Groups (fig. 6). This supports that these grains are sourced by the CMC, which provided metamorphically overprinted material from the Orca and Valdez Groups that formed simultaneously with the SBPB.

The $\varepsilon(\mathrm{Hf})_t$ values of group 3 (>60 Ma) overlap in age and $\varepsilon(\mathrm{Hf})_t$ the Orca and Yakutat Groups and the CPC (fig. 6; Garver and Davidson 2015), supporting the provenance indicated by the U-Pb age spectra. Parts of the Orca Group were deposited shortly before, during, or after the emplacement of the SBPB (<70 Ma) and show $\varepsilon(\mathrm{Hf})_t$ values similar to those of the plutons of the SBPB. This causes some overlap of $\varepsilon(\mathrm{Hf})_t$ values and U-Pb ages for the two groups. The absence of $\varepsilon(\mathrm{Hf})_t$ data for the Poul Creek, Kulthieth, and Yakataga Formations and the Valdez Group precludes comparison with these sources.

Provenance Affiliations of REEs. The REE spectra of zircons have been found to be not directly indicative for provenance (Hoskin 2003). Still, certain shapes and slopes of chondrite-normalized REE patterns are characteristic for certain rock types and can help to link detrital grains to certain source lithologies (Rowley et al. 1997; Belousova et al. 2002; Hoskin 2003; Grimes et al. 2007; Rubatto 2017). Inherited cores like those found in zircons of the CMC give information on ancestral sources (Belousova et al. 2002).

The REE spectra of zircons from site U1417 and U1418 samples with different depositional ages show similar patterns (fig. 7). Therefore, a contribution of all zircons from a provenance with similar lithologies is likely. There is no correlation between zircon ages and REE spectra. Zircon REE literature data from the possible source areas are rare. There is one data set from Gasser et al. (2012) that provides REE spectra of zircons from a granodiorite within the CMC that strongly resemble the majority of REE spectra found in our samples in shape and element concentrations. This agrees with a contribution of most of the ca. 50–60 Ma zircons from the granodiorites of the SBPB within the Chugach/Yakutat area. Some grains have a very low Ce anomaly and low to pronounced Eu anomalies and do not match this pattern. They may have a more granitic source, according to Belousova et al. (2002). For the older grains, a granodioritic to granitic source is in line with the proposed source of the flysch sediments in the CPC (Perry et al. 2009).

Provenance Affiliations of (U-Th)/He Data. Fission-track and (U-Th)/He dating provides information on cooling histories of zircons (Hurford and Carter 1991; Reiners 2005). Both methods have been widely used to unravel the orogenic history of southern Alaska (Berger et al. 2008*a*, 2008*b*; Berger and Spotila 2008; Enkelmann et al. 2008, 2010, 2015, 2017; Falkowski et al. 2014, 2016; Dunn et al. 2017). Wide parts of the southern Alaska margin underwent different events of metamorphism that resulted in diverse degrees of heating, causing varying degrees of resetting of the low-temperature thermochronological system (Plafker 1987; Plafker et al. 1994; Berger et al. 2008*b*; Berger and Spotila 2008; Enkelmann et al. 2010; Gasser et al. 2011; Carlson 2012). All the different signals (reset, unreset, partial reset) that are stored in the source rocks are mixed in the site U1417 and U1418 sediments and complicate the interpretation of the thermochronological data. Because of the close range of zircon FT (ZFT) and ZHe closure temperatures (ca. 190°–270°C and 130°–260°C, respectively; Reiners 2005), these thermochronometers yield similar age components. We compare the main age components registered in our samples with the respective literature data obtained for the source rocks onshore: the Orca and Valdez Groups, the Poul Creek and Kulthieth Formations, and the SBPB and CMC, as well as the coeval Yakataga Formation.

Zircon (U-Th)/He cooling ages of ca. 3–154 Ma have been found in the Chugach–Prince William terrane. Three thermal events have been identified for the western Orca and Valdez Groups: a ~50 Ma event caused by the intrusions of the SBPB, a second phase of plutonism at ~38 Ma, and a 25–30 Ma cooling event that is considered to have been caused by the collision of the Yakutat microplate and subsequent exhumation in the evolving mountain belt (Carlson 2012). Within the Orca Group, these events caused different histories of heating, leading to locally varying degrees of resetting of geochronological systems (Carlson 2012). Within the CMC, temperatures were high enough to reset all low-temperature thermochronological systems (Gasser et al. 2011, 2012). The western and central parts of the CMC cooled relatively rapidly from 55 to 52 Ma, at rates of 29°–180°C/My (Gasser et al. 2011). This was followed by further rapid cooling to nearly surface temperatures in the Eocene. Contrastingly, in areas to the south, temperatures remained at ca. 300°–400°C for 15–20 My and cooled through FT closure temperature at ca. 30–25 Ma (Gasser et al. 2011). In the eastern part of the CMC, cooling was slow and reached 200°–300°C at ca. 5 Ma (Gasser et al. 2011). Cooling rates increased again during the past ~5 My to rates of 20°–40°C/My (Gasser et al. 2011).

The Poul Creek and Kulthieth Formations might have locally experienced resetting of apatite (U-Th-Sm)/He, ZHe, apatite FT, and ZFT ages (Perry et al. 2009). Main ZFT age components have been found at 29 Ma (37%), 41 Ma (52%), and 63 Ma (11%) for the Poul Creek Formation and at 28 Ma (27%), 39 Ma (65%), and 78 Ma (8%) for the Kulthieth Formation (Perry et al. 2009).

The (U-Th)/He cooling ages of the plutons of the SBPB also decrease from west to east, starting with 37 Ma for the Sanak Island pluton, ~33 Ma for the

Eagle Harbor pluton on Kodiak Island, ~29 Ma for the Aialik pluton near Seward, and ~16 Ma for the Crawfish Inlet pluton on Baranof Island (Schneider et al. 2015).

Comparison with our data shows that cooling ages of roughly ~50–96, ~33–45, and ~25 –30 Ma in the Orca and Valdez Groups and the Kulthieth and Poul Creek Formations cover the main age components found within the site U1417 and U1418 sediments (table 2). They also overlap the ZHe ages of ca. 36–65 Ma found north of the Border Ranges fault (Enkelmann et al. 2017). The cooling ages of the plutons of the SBPB and the cooling histories of the western and central CMC match the two most prominent age components in the site U1417 samples, at ca. 24 and 44 Ma. This complicates the discrimination of different sources.

A detailed study of the Yakataga Formation, deposited at the same time as the Surveyor Fan sediments, showed four main FT age components, at ca. ~8 Ma (~5%), ~15–17 Ma (~40%), ~21–35 Ma (~30%–50%), and 68–77 Ma (11%–30%; Perry et al. 2009). Excepting the 15–17 Ma population, all the older components were found to be statistically identical to the age components found within the underlying Poul Creek and Kulthieth Formations (Perry et al. 2009). This implies that the Yakataga sediments consist of reworked material from the Poul Creek and Kulthieth Formations and an additional source, delivering mainly 17 and 25 Ma cooling-age components, that is very likely the Chugach terrane (Perry et al. 2009). Perry et al. (2009) found 65% of the Yakutat Formation to be sourced by the CMC and SBPB, while about 35% could be ascribed to recycling of the Poul Creek and Kulthieth Formations. The youngest age component, 24 ± 8 Ma (ca. 70%), of the Miocene site U1417 sediments covers the range of the two youngest age components of the Yakataga Formation, indicating similar sources. The proportions of the different age components have to be interpreted carefully, because they are strongly affected by counting statistics. However, the agreement between our (U-Th)/He age spectra and those from the Yakataga Formation support evidence that the (U-Th)/He data are, in turn, compatible with our U-Pb age data.

Together with the U-Pb ages that imply ca. 60% input from the CMC and SBPB for sample 17Mi1, the provenance of these sediments and the Yakataga Formation is very likely the same. The large fraction of zircons sourced by the CMC and SBPB in samples 17Mi1 and 17Mi2 implies high erosion rates in these areas in the Miocene (ca. 7–10 Ma), compared to the surrounding areas. The Pliocene sample shows fewer grains of the two young populations (ca. 2%). The analysis of the U-Pb ages indicates a reduced transfer of material from the CMC and the SBPB (44%), mainly because less material was provided by the CMC. This implies a change in provenance to more input from the low- and nonmetamorphic parts outside the CMC area.

Provenance Implications of the Data

Our U-Pb age data (fig. 5*A*–5*H*) do not show the limited range of ages identified by Dunn et al. (2017). These authors found only a limited range of ages between 85 and 50 Ma in samples from 617 m CCSF-B at site U1417. We conclude that the major sediment sources remained the same throughout the Miocene, albeit with changes in relative contribution. In the MDS plot (fig. 10), the Miocene samples from site U1417 plot closer to the reference data from the plutons than all other samples. They also plot very close to sample UT46 (CMC) and have relatively high fractions of group 2 zircons, indicating that they experienced higher input from the SBPB and the CMC than all other samples. With younger depositional age, both the similarity to the reference samples from the SBPB and the CMC and the fraction of group 1 and 2 zircons decrease (figs. 9, 10). We interpret this as a decrease in the input from the CPC and the CMC. This, in turn, implies rising input from the low- or unmetamorphosed lithologies exposed on the seaward slopes of the mountain range.

From the Pleistocene onward, the input from non-CMC/SBPB grains seems to be relatively constant (figs. 9, 10). The Pliocene sample from site U1417 and all middle Pleistocene samples from site U1418 form a dense cloud in the MDS plot, together with the Yakataga Formation, supporting their similarity. Furthermore, they plot in the middle of all reference samples, indicating them to be a mixture of all. The Pleistocene sample from site U1417 plots close to the CPC and the Poul Creek Formation, but the low grain number lowers the significance. The middle Pleistocene sediments from site U1418 show high fractions of group 3 zircons, implying high input from sources close to the coast.

Sample 18EPl (MTD) differs from the other Pleistocene samples (figs. 9, 10). In the MDS plot, it plots close to samples from the Yakutat terrane that were taken close to the Bering glacier (fig. 10). These samples have a drainage area underlain by the Yakataga and Poul Creek Formations (Enkelmann et al. 2008). They are suggested to have been fed by rapidly exhuming ice-covered rocks (Bagley icefield and Seward glacier) ca. ~50–200 km east of the syntaxis region (Enkelmann et al. 2008). We therefore suggest this sample to have been fed nearly exclusively through the Bering glacier supplying high amounts

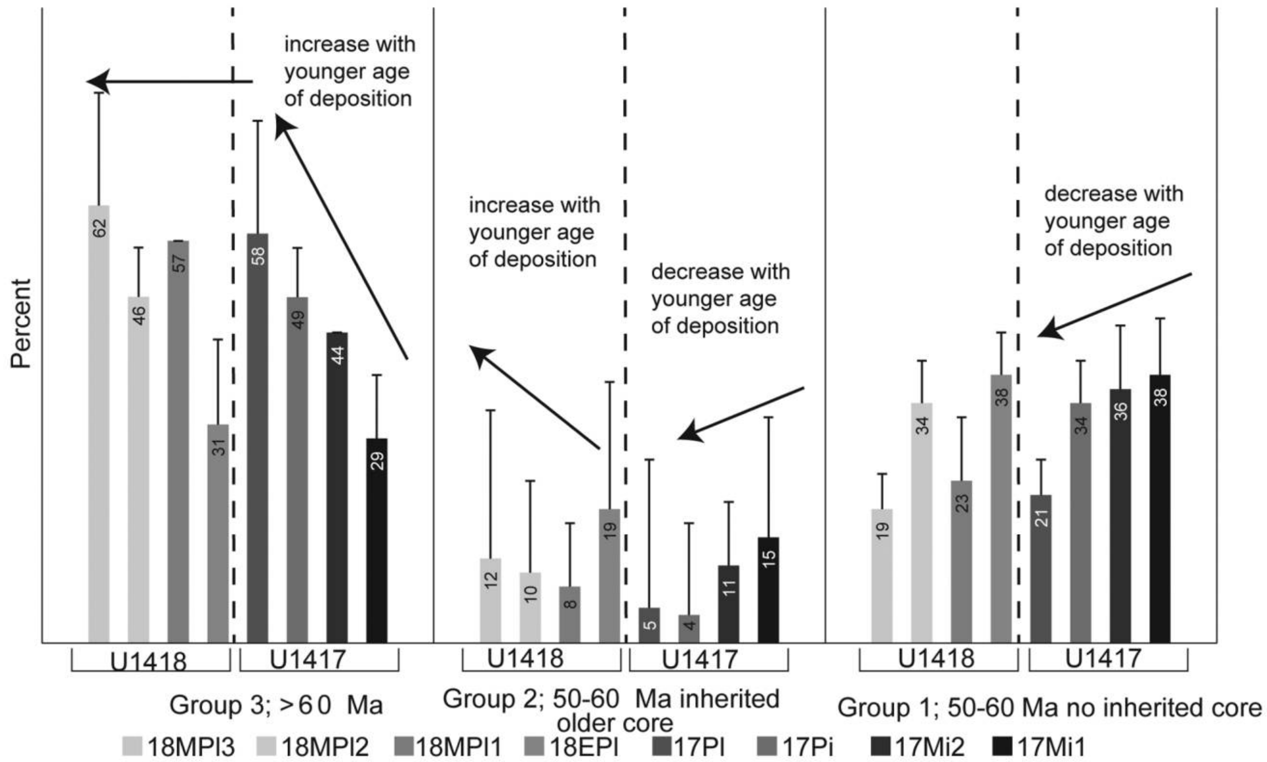

Figure 9. Relative abundances of zircons from Miocene to Pleistocene sediments from sites U1417 and U1418 of U-Pb age groups 1–3. A color version of this figure is available online.

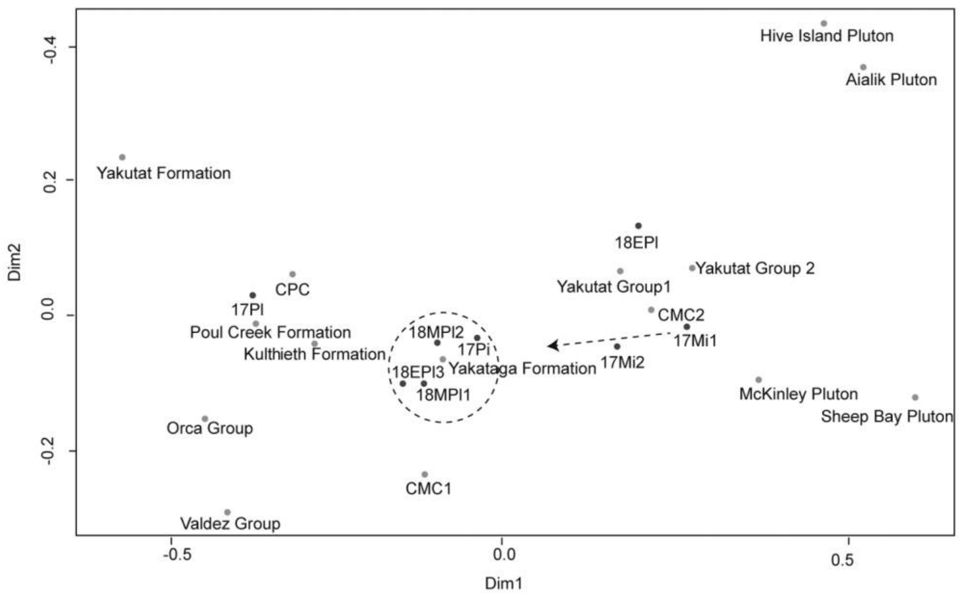

Figure 10. Multidimensional scaling plot for the samples of this study (names beginning with 17 or 18) and from the Valdez, Orca, and Yakutat Groups; the Kulthieth, Poul Creek, and Yakataga Formations; the Coast Plutonic Complex (CPC); and the Chugach Metamorphic Complex (CMC; from Enkelmann et al. 2008; Gehrels et al. 2009; Perry et al. 2009; Garver and Davidson 2015). The dashed circle highlights grouping of samples from site U1418 and sample 17Pi. The dashed arrow highlights increasing similarity of samples from site U1417 with younger depositional age. A color version of this figure is available online.

of material from the CMC, which is also supported by the absence of grains older than 264 ± 4 Ma.

Exhumation Rates

Rising exhumation rates during the Miocene have been deduced from site U1417 sediments on the basis of ZFT data from two samples from ca. 617 m CCSF-B (the same depth interval where we took sample 17Mi2; 603 m CCSF-B) and 700 m CCSF-B (Dunn et al. 2017). The samples were inferred to have depositional ages of 8 and 10 Ma, respectively (Dunn et al. 2017). They calculated an exhumation rate of 2.8 ± 1.0 km/My (lag time of 1.6 ± 0.2 My) for the sample from ca. 617 m CCSF-B (Dunn et al. 2017). We found a (U-Th)/He zircon aged 6.9 ± 0.7 Ma in sample 17Mi2 that has a depositional age of ca. 7.4–8 Ma, according to Expedition 341 Scientists (2014). This indicates that this sediment is not older than 7.6 Ma but very likely younger. When the exhumation rates are recalculated with a deposition age of 7 Ma (resulting in a lag time of ca. 2.6 ± 0.2 My) and the same one-dimensional steady-state thermal model used by Dunn et al. (2017; also see Campbell et al. 2005; Reiners and Brandon 2006), exhumation appears to have been slower, at ca. 2.1 km/My. Regarding the high uncertainty of the depositional age of the sample, which Dunn et al. (2017) supposed to be 10 Ma but, according to Expedition 341 Scientists (2014), might be as high as 13 Ma, exhumation rates at that time could theoretically be as high as ca. 5 km/My. Considering the whole range of possible exhumation rates for the two Miocene samples, the error on the exhumation rates caused by the analytical error of age determination and the error on the depositional age is too large to support the suggested increase in exhumation rates in the Miocene.

Discussion

Miocene. The presence of grains in the Miocene sediments that can be attributed to the CMC suggest sediment transport from sources as far northwestward as the position of the CMC to the Surveyor Fan in the Miocene. Transport of the orogenic detritus into the fan can be inferred to be geologically instantaneous because of the short transport distance (Dunn et al. 2017). Exhumation in the area of the CMC has been going on since the Oligocene to mid-Miocene as a result of transpressive strike-slip movement of the Yakutat terrane, followed by its collision with the North American continent since the mid-Miocene (Spotila and Berger 2010; Falkowski et al. 2014, 2016; Enkelmann et al. 2017). The depositional age of the oldest sample corresponds to an exhumation phase of the Chugach terrane at ca. 11 ± 2 Ma, caused by changes in plate motion and subduction style and the final collision of the Yakutat terrane (Enkelmann et al. 2008). Furthermore, deep-seated and rapid exhumation of the St. Elias syntaxis started at ca. ~11–8 Ma, and thermochronologic data imply input from there to the distal site at 8 Ma (Dunn et al. 2017). The deep-seated erosion is considered to result from coupling between erosion and active tectonic rock uplift (Enkelmann et al. 2009, 2017; Falkowski et al. 2016; Dunn et al. 2017). Enkelmann et al. (2017) suggest that a fluvial system existed, allowing tectonics and erosion to cause rapid exhumation even before the onset of glaciation. A hypothetical channel system delivering material from northward sources is favored by southward thinning of seismic reflectors within the Miocene precursor of the Surveyor Fan (Stevenson and Embley 1987). These channels might have drained the hypothetical onshore fluvial system, delivering material from the CMC into the Gulf of Alaska and to the Miocene Surveyor Fan.

Miocene to Pliocene. Our data imply increasing erosion in the low-grade metamorphic areas closer to the coast during the Miocene and Pliocene. This is also supported by single-grain heavy-mineral provenance analysis (Huber et al. 2018). Three main areas of erosion have been identified at the southern Alaska continental margin: (1) the syntaxis area, especially under the Seward glacier, (2) along the Fairweather fault, and (3) in the fold-and-thrust belt (Enkelmann et al. 2009, 2010). The high rates of exhumation found for the St. Elias syntaxis (fig. 1*B*) are interpreted to be the result of effective coupling of glacial erosion and uplift through tectonic processes at the plate corner (Spotila and Berger 2010; Enkelmann et al. 2015).

The impact of climate versus tectonic factors on exhumation at the southern Alaska continental margin is a subject of the ongoing research (e.g., Berger et al. 2008*a*, 2008*b*; Berger and Spotila 2008; Enkelmann et al. 2009, 2010, 2015, 2017; Headley et al. 2012, 2013; Pavlis et al. 2012; Gulick et al. 2015). Some authors emphasize the impact of the glacial system (Berger et al. 2008*a*, 2008*b*; Pavlis et al. 2012; Gulick et al. 2015); others highlight the interaction of the two (Spotila et al. 2004; Meigs et al. 2008; Enkelmann et al. 2009, 2017; Headley et al. 2012, 2013) or the limited impact of the glaciation (Enkelmann et al. 2010). Reactivation of the Contact fault at ca. 6–5 Ma, caused by the final collision of the Yakutat terrane and dextral transpression associated with lens-like pop-up structures, is suggested to have resulted in locally very rapid exhumation along that fault and in the accretionary wedge (Enkelmann et al. 2008). Bedrock apatite ages are very young (4–0.5 Ma) in the fold-and-thrust belt and the Yakutat Foothills and along the Fairweather fault and show Pliocene ZHe and ZFT ages (Enkelmann et al. 2010). In addition, the decreasing input from the CMC from the Miocene to the Pliocene correlates with the southward progress of glaciers from the interior of the evolving mountain belt toward the ocean. Having started in the Miocene, this trend is even stronger at the transition from the Miocene to the Pliocene, with the onset of tidewater glaciation. Strong glacial erosion since the end of the Miocene is considered to have led to erosion focusing on windward positions, correlating with the equilibrium line altitude (Spotila et al. 2004; Berger et al. 2008*a*, 2008*b*; Meigs et al. 2008). This is in line with erosion increasing in the areas closer to the coast. This implies that glacial erosion and sediment evacuation are much more efficient in the areas close to the coast than in the interior parts of the orogen (e.g., Berger et al. 2008*a*, 2008*b*; Spotila and Berger 2010). Glaciation and tectonic processes seem to have interacted in determining the changing provenance signal connected to the evolving main erosion centers, which is also inferred from single-grain heavy-mineral analysis (Huber et al. 2018). However, our data set does not allow for differentiation of the relative contributions of tectonics and climate.

Pleistocene. Low numbers of zircons in the Pleistocene samples at the distal site (U1417) and the different geographic position of the proximal site (U1418) on the upper Surveyor Fan and away from the Surveyor channel complicate the comparison to the Miocene and Pliocene deposits of site U1417. Previous studies have revealed that the Bering-Bagley glacial system and the Malaspina glacier drain different catchments, with only the former delivering material from the syntaxis (Enkelmann et al. 2009; Dunn et al. 2017). Parallel transport paths of sediments below the Malaspina glacier prevent mixing and result in variations in the FT age spectra within the Malaspina lobe (Enkelmann et al. 2009). This emphasizes the strong impact of glacial sediment routing on provenance.

The proximal site U1418 very likely experienced input directly from the Bering-Bagley glacial system, while the distal site U1417 was fed by a much wider part of the continental margin through the Surveyor Channel and its tributaries. Accordingly, the proximal site records more-local processes affecting its catchment (Expedition 341 Scientists 2014; Dunn et al. 2017; Huber et al. 2018). The early Pleistocene sample from site U1418, which differs from the other Pleistocene samples, represents MTDs very likely connected to a major slope failure (Reece et al. 2011). Of all samples, this one shows the highest amount of material sourced by the CMC. This rather reflects a single extreme event and is not the result of changing erosion patterns.

Before the MPT, denudation rates in the subaerial parts of the orogenic wedge are supposed to have been relatively low (35 km^2/My unit flux; Berger et al. 2008*a*). During the Pleistocene and especially after the MPT, denudation increased strongly, resulting in denudation rates of ca. 190 km^2/My unit flux (Berger et al. 2008*a*). At the same time, sedimentation rates of the Surveyor Fan increased markedly (Gulick et al. 2015).

The scarcity of zircons in the Pleistocene sediments at the distal site limits a detailed evaluation of the provenance evolution. Still, the middle Pleistocene sediments from the proximal site have a provenance similar to that of the Pliocene/late Miocene samples from the distal site, irrespective of the different locations of the sites. As the proximal site did not receive input from the syntaxis (Dunn et al. 2017), we cannot provide information on how the syntaxis might have been affected by changes at the MPT. However, the increased glaciation since the MPT has been found to have not affected tectonic processes within the syntaxis area (Enkelmann et al. 2010).

Our data from the distal site suggest that high erosion rates in the fold-and-thrust belt were not initiated during the MPT. They had already started to develop during the Miocene-Pliocene transition at a time of increasing glaciation. The findings of this study combine well with several aspects of climate-tectonic interactions concurring in the Chugach–St. Elias orogeny. These are (1) the strong correlation of rising sedimentation rates in the Surveyor Fan and increasing glaciation of the southern Alaska continental margin (Gulick et al. 2015) and (2) enhanced erosion at the windward side of the orogen (e.g., Pewé 1975; Berger et al. 2008*a*), denudation patterns being strongly influenced by the location of glaciers (Spotila et al. 2004). We conclude that climate and glacial erosion have strongly affected erosion patterns in the Chugach–St. Elias orogen since the onset and intensification of glaciation at the Miocene-Pliocene boundary.

Our data from the proximal site do not evince a general change in the tectonic pattern after the MPT. This may be an effect of the methods applied and may not necessarily be suggestive of the absence of such a change. As the response time of orogens to changing climatic and tectonic forces varies strongly (Tomkin and Roe 2007), changes since the MPT might be too recent to be effectively detected in the Surveyor Fan sediments. Determination of exhumation rates for the Pleistocene through low-temperature thermochronology of the Surveyor Fan sediments is not possible for the Chugach–St. Elias orogen because of a lag time of several million years (Dunn et al. 2017). At present, it cannot be decided whether the observed changes reflect variations in the rates of sediment removal or exhumation.

Conclusion

Our multimethod zircon data identify the main sediment sources of the Surveyor Fan to be located on the Chugach and Yakutat terranes since the Miocene. Additional input from the CPC cannot be ruled out. Even during enhanced glaciation in the Pleistocene, glaciers seem to have been nested in the same area as before, providing zircons with similar characteristics. Our data favor sediment input from the CMC to the Surveyor Fan during Miocene time (ca. 11 Ma). Transport during the Miocene to the Surveyor Fan may have occurred via a channel system that has already been subducted in the Aleutian Trench (Stevenson and Embley 1987). Thermochronological data support that exhumation rates in the Miocene were more or less constant; the large errors on the depositional ages and the thermochronological data might mask small variations.

From the Miocene-Pliocene boundary onward, the advance of glaciers toward the Gulf of Alaska, as well as tectonics, has focused erosion along the spine of the orogen. The absence of zircons in the Pleistocene sediments at the distal site U1417 hampers a comparison of the provenance of the Miocene-Pliocene and Pleistocene sediments. Still, our data from the proximal site imply a constant sediment provenance over the MPT, indicating that the main erosion centers have remained the same. The similarity of age distributions and geochemical compositions of zircons from different source areas along the Gulf of Alaska, as well as the transfer times of tectonic events recorded in the Surveyor Fan sediments, may mask local changes in the Pleistocene.

ACKNOWLEDGMENTS

This study was funded by German Research Foundation (DFG) grants BA 1011/43-1 and 43-2. We thank M. Dröllner, of Münster, for helping to process the samples and B. Schmitte, of Münster, for assistance with acquiring the microprobe and LA-ICP-MS data. We thank P. Wilde, of Berkeley, for revising the English text. We thank E. Enkelmann and an anonymous reviewer for their constructive reviews and D. Rowley for editorial guidance.

REFERENCES CITED

Amelin, Y.; Lee, D. C.; and Halliday, A. N. 2000. Early-middle Archaean crustal evolution deduced from Lu-Hf and U-Pb isotopic studies of single zircon grains. Geochim. Cosmochim. Acta 64:4205–4225.

Arkle, J. C.; Armstrong, P. A.; Haeussler, P. J.; Prior, M. G.; Hartman, S.; Sendziak, K. L.; and Brush, J. A. 2013. Focused exhumation in the syntaxis of the western Chugach Mountains and Prince William Sound, Alaska. Geol. Soc. Am. Bull. 125:776–793.

Armstrong, R. L. 1988. Mesozoic and early Cenozoic magmatic evolution of the Canadian Cordillera. *In* Clark, S. P., Jr.; Burchfiel, B. C.; and Suppe, J., eds. Processes in continental lithospheric deformation. Geol. Soc. Am. Spec. Pap. 218:55–92.

Arntson, E.; Olson, H.; Davidson, C.; and Garver, J. 2017. Geochemistry, U-Pb ages, and Hf isotopes of the Mt. Draper and Mt. Stamy plutons, Nunatak fjord, Alaska: implications for the Sanak-Baranof Plutonic Belt. Geol. Soc. Am. Abstr. Program 49(4). doi:10.1130/abs/2017CD-292866.

Barker, F.; Farmer, G. L.; Ayuso, R. A.; Plafker, G.; and Lull, J. S. 1992. The 50 Ma granodiorite of the eastern Gulf of Alaska: melting in an accretionary prism in the forearc. J. Geophys. Res. 97(B5):6757–6778.

Belousova, E.; Griffin, W.; O'Reilly, S. Y.; and Fisher, N. 2002. Igneous zircon: trace element composition as an indicator of source rock type. Contrib. Mineral. Petrol. 14:602–622.

Berger, A. L.; Gulick, S. P. S.; Spotila, J. A.; Upton, P.; Jaeger, J. M.; Chapman, J. B.; Worthington, L. A.; et al. 2008*a*. Quaternary tectonic response to intensified glacial erosion in an orogenic wedge. Nat. Geosci. 1:793–799.

Berger, A. L., and Spotila, J. A. 2008. Denudation and deformation in a glaciated orogenic wedge: the St. Elias orogen, Alaska. Geology 36:523–526.

Berger, A. L.; Spotila, J. A.; Chapman, J. B.; Pavlis, T. L.; Enkelmann, E.; Ruppert, N. A.; and Buscher, J. T. 2008*b*. Architecture, kinematics, and exhumation of a convergent orogenic wedge: a thermochronological investigation of tectonic-climatic interactions within the central St. Elias orogen, Alaska. Earth Planet. Sci. Lett. 270:13–24.

Botev, Z. I.; Grotowski, J. F.; and Kroese, D. P. 2010. Kernel density estimation via diffusion. Ann. Statist. 38:2916–2957.

Bradley, D. C.; Haeussler, P. J.; and Kusky, T. M. 1993. Timing of early Tertiary ridge subduction in southern Alaska. *In* Dusel-Bacon, C., and Till, A. B., eds. Geologic studies in Alaska by the U.S. Geological Survey. U.S. Geol. Surv. Bull. 2068:163–177.

Bradley, D. C.; Kusky, T. M.; Haeussler, P. J.; Goldfarb, R. J.; Miller, M. L.; Dumoulin, J. A.; Nelson, S. W.; and Karl, S. M. 2003. Geologic signature of early Tertiary ridge subduction in Alaska. *In* Sisson, V. B.; Roeske, S. M.; and Pavlis, T. L., eds. Geology of a transpressional orogen developed during ridge-trench interaction along the North Pacific margin. Geol. Soc. Am. Spec. Pap. 371:19–49.

Bruand, E.; Gasser, D.; Bonnand, P.; and Stuewe, K. 2011. The petrology and geochemistry of a metabasite belt along the southern margin of Alaska. Lithos 127:282–297.

Bruand, E.; Gasser, D.; and Stüwe, K. 2014. Metamorphic *P-T* conditions across the Chugach Metamorphic Complex (Alaska)—a record of focused exhumation during transpression. Lithos 190–191:292–312.

Bruhn, R. L.; Sauber, J.; Cotton, M. M.; Pavlis, T. L.; Burgess, E.; Ruppert, N.; and Forster, R. R. 2012. Plate margin deformation and active tectonics along the northern edge of the Yakutat Terrane in the Saint Elias Orogen, Alaska, and Yukon, Canada. Geosphere 8:1384–1407.

Bruns, T. R. 1983. Model for the origin of the Yakutat terrane, an accreting terrane in the northern Gulf of Alaska. Geology 11:718–721.

Campbell, I. H.; Reiners, P. W.; Allen, C. M.; Nicolescu, S.; and Upadhyay, R. 2005. He-Pb double dating of detrital zircons from the Ganges and Indus Rivers: implication for quantifying sediment recycling and provenance studies. Earth Planet. Sci. Lett. 237:402–432.

Carlson, B. M. 2012. Analysis of detrital zircon fission track ages of the Upper Cretaceous Valdez Group and Paleogene Orca Group in western Prince William Sound, Alaska. *In* Varga, R. J., ed. Keck Geology Consortium Undergraduate Research Symposium, 25th (Amherst, MA, 2012), Proc. Claremont, CA, Geol. Dept., Pomona College, p. 8–16.

Carlson, P. R.; Stevenson, A. J.; Bruns, T. R.; Mann, D. M.; and Huggett, Q. 1996. Sediment pathways in Gulf of Alaska from beach to abyssal plain. *In* Gardner, J. V.; Field, M. E.; and Twichell, D. C., eds. Geology of the United States seafloor: the view from GLORIA. Cambridge, Cambridge University Press, p. 255–278.

Cecil, M. R.; Gehrels, G.; Ducea, M. N.; and Patchett, P. J. 2011. U-Pb-Hf characterization of the central Coast Mountains batholith: implications for petrogenesis and crustal architecture. Lithosphere 3:247–260.

Cherniak, D. J., and Watson, E. B. 2001. Pb diffusion in zircon. Chem. Geol. 172:5–24.

Colpron, M., and Nelson, J. L. 2011. A digital atlas of terranes for the Northern Cordillera. Whitehorse, Yukon Geological Survey. www.geology.gov.yk.ca. Accessed March 15, 2018.

Colpron, M.; Nelson, J. L.; and Murphy, D. C. 2007. Northern Cordilleran terranes and their interactions through time. GSA Today 17:4–10.

Cowan, D. S. 2003. Revisiting the Baranof–Leech River hypothesis for early Tertiary coastwise transport of the Chugach–Prince William terrane. Earth Planet. Sci. Lett. 213:463–475.

Davidson, C., and Garver, J. I. 2017. Age and origin of the Resurrection ophiolite and associated turbidites of the Chugach–Prince William Terrane, Kenai Peninsula, Alaska. J. Geol. 125:681–700.

Dobson, M. R.; O'Leary, D.; and Veart, M. 1998. Sediment delivery to the Gulf of Alaska: source mechanisms along a glaciated transform margin. *In* Stoker, M. S.; Evans, D.; and Cramp, A., eds. Geological processes on continental margins: sedimentation, mass-wasting and stability. Geol. Soc. Lond. Spec. Publ. 129:43–66.

Dodds, C. J., and Campbell, P. B. 1988. Potassium-argon ages of mainly intrusive rocks in the Saint Elias Mountains, Yukon and British Columbia. Geol. Surv. Can. Pap. 87-16, 43 p.

Dumoulin, J. 1987. Sandstone composition of the Valdez and Orca groups, Prince William Sound, Alaska. U.S. Geol. Surv. Bull. 1774, 37 p.

Dunkl, I., and Székely, B. 2002. Component analysis with visualization of fitting—PopShare, a Windows program for data analysis. Geochim. Cosmochim. Acta 66 (Suppl. 1):A201.

Dunn, C. A.; Enkelmann, E.; Ridgway, K. D.; and Allen, W. K. 2017. Source to sink evaluation of sediment routing in the Gulf of Alaska and southeast Alaska: a thermochronometric perspective. J. Geophys. Res. Earth Surf. 122:711–734.

Eberhart-Phillips, D.; Christensen, D. H.; Brocher, T. M.; Hansen, R.; Ruppert, N. A.; Haeussler, P. J.; and Abers, G. A. 2006. Imaging the transition from Aleutian subduction to Yakutat collision in central Alaska, with local earthquakes and active source data. J. Geophys. Res. 111:B11303. doi:10.1029/2005JB004240.

Elliott, J. L.; Larsen, C. F.; Freymueller, J. T.; and Motyka, R. J. 2010. Tectonic block motion and glacial isostatic adjustment in southeast Alaska and adjacent Canada constrained by GPS measurements. J. Geophys. Res. 115:B09407. doi:10.1029/2009JB007139.

Enkelmann, E.; Garver, J. I.; and Pavlis, T. L. 2008. Rapid exhumation of ice-covered rocks of the Chugach–St. Elias orogen, southeast Alaska. Geology 36:915–918.

Enkelmann, E.; Koons, P. O.; Pavlis, T. L.; Hallet, B.; Barker, A.; Elliott, J.; Garver, J. I.; et al. 2015. Cooperation among tectonic and surface processes in the St. Elias Range, Earth's highest coastal mountains. Geophys. Res. Lett. 42:5838–5846.

Enkelmann, E.; Piestrzeniewicz, A.; Falkowski, S.; Stübner, K.; and Ehlers, T. A. 2017. Thermochronology in southeast Alaska and southwest Yukon: implications for North American plate response to terrane accretion. Earth Planet. Sci. Lett. 457:348–358.

Enkelmann, E.; Zeitler, P. K.; Garver, J. I.; Pavlis, T. L.; and Hooks, B. P. 2010. The thermochronological record of tectonic and surface process interaction at the Yakutat–North American collision zone in southeast Alaska. Am. J. Sci. 310:231–260.

Enkelmann, E.; Zeitler, P. K.; Pavlis, T. L.; Garver, J. I.; and Ridgway, K. D. 2009. Intense localized rock uplift and erosion in the St Elias orogen of Alaska. Nat. Geosci. 2:360–363.

Expedition 341 Scientists. 2014. Southern Alaska margin: interactions of tectonics, climate, and sedimentation. Integrated Ocean Drilling Program Expedition 341 Prelim. Rep. doi:10.2204/iodp.pr.341.2014.

Falkowski, S., and Enkelmann, E. 2016. Upper-crustal cooling of the Wrangellia composite terrane in the northern

St. Elias Mountains, western Canada. Lithosphere 8:359–378.

Falkowski, S.; Enkelmann, E.; Drost, K.; Pfänder, J. A.; Stübner, K.; and Ehlers, T. A. 2016. Cooling history of the St. Elias syntaxis, southeast Alaska, revealed by geochronology and thermochronology of cobble-sized glacial detritus. Tectonics 35:447–468.

Falkowski, S.; Enkelmann, E.; and Ehlers, T. A. 2014. Constraining the area of rapid and deep-seated exhumation at the St. Elias syntaxis, southeast Alaska, with detrital zircon fission-track analysis. Tectonics 33:597–616.

Farris, D. W.; Haeussler, P.; Friedman, R.; Paterson, S. R.; Saltus, R. W.; and Ayuso, R. 2006. Emplacement of the Kodiak batholith and slab-window migration. Geol. Soc. Am. Bull. 118:1360–1376.

Farris, D. W., and Paterson, S. R. 2009. Subduction of a segmented ridge along a curved continental margin: variations between the western and eastern Sanak-Baranof belt, southern Alaska. Tectonophysics 464:100–117.

Finzel, E. S.; Trop, J. M.; Ridgway, K. D.; and Enkelmann, E. 2011. Upper plate proxies for flat-slab subduction processes in southern Alaska. Earth Planet. Sci. Lett. 303: 348–360.

Fuis, G. S.; Moore, T. E.; Plafker, G.; Brocher, T. M.; Fisher, M. A.; Mooney, W. D.; Nokleberg, W. J.; et al. 2008. Trans-Alaska crustal transect and continental evolution involving subduction underplating and synchronous foreland thrusting. Geology 36:267–270.

Garver, J. I., and Davidson, C. M. 2015. Southwestern Laurentian zircons in Upper Cretaceous flysch of the Chugach-Prince William terrane in Alaska. Am. J. Sci. 315:537–556.

Gasser, D.; Bruand, E.; Stüwe, K.; Foster, D. A.; Schuster, R.; Fügenschuh, B.; and Pavlis, T. 2011. Formation of a metamorphic complex along an obliquely convergent margin: structural and thermochronological evolution of the Chugach Metamorphic Complex, southern Alaska. Tectonics 30:TC2012. doi:10.1029/2010TC002776.

Gasser, D.; Rubatto, D.; Bruand, E.; and Stüwe, K. 2012. Large-scale, short-lived metamorphism, deformation, and magmatism in the Chugach metamorphic complex, southern Alaska: a SHRIMP U-Pb study of zircons. Geol. Soc. Am. Bull. 124:886–905.

Gehrels, G.; Rusmore, M.; Woodsworth, G.; Crawford, M.; Andronicos, C.; Hollister, L.; Patchett, J.; et al. 2009. U-Th-Pb geochronology of the Coast Mountains batholith in north-coastal British Columbia: constraints on age and tectonic evolution. Geol. Soc. Am. Bull. 121:1341–1361.

Gehrels, G. E. 2014. Detrital zircon U-Pb geochronology applied to tectonics. Annu. Rev. Earth Planet. Sci. 42: 127–149.

Grabowski, D. M.; Enkelmann, E.; and Ehlers, T. A. 2013. Spatial extent of rapid denudation in the glaciated St. Elias syntaxis region, SE Alaska. J. Geophys. Res. Earth Surf. 118:1921–1938.

Grimes, C. B.; John, B. E.; Kelemen, P. B.; Mazdab, F. K.; Wooden, J. L.; Cheadle, M. J.; Hanghøj, K.; and Schwartz, J. J. 2007. Trace element chemistry of zircons from oceanic crust: a method for distinguishing detrital zircon provenance. Geology 35:643–646.

Gulick, S. P. S.; Jaeger, J. M.; Mix, A. C.; Asahi, H.; Bahlburg, H.; Belanger, C. L.; Berbel, G. B. B.; et al. 2015. Mid-Pleistocene climate transition drives net mass loss from rapidly uplifting St. Elias Mountains, Alaska. Proc. Natl. Acad. Sci. USA 112:15,042–15,047.

Haeussler, P. J.; Bradley, D. C.; Wells, R. E.; and Miller, M. L. 2003. Life and death of the Resurrection plate: evidence for its existence and subduction in the northeastern Pacific in Paleocene-Eocene time. Geol. Soc. Am. Bull. 115:867–880.

Harris, N. R.; Sisson, V. B.; Wright, J. E.; and Pavlis, T. L. 1996. Evidence for Eocene mafic underplating during fore-arc intrusive activity, eastern Chugach Mountains, Alaska. Geology 24:263–266.

Headley, R.; Hallet, B.; Roe, G.; Waddington, E. D.; and Rignot, E. 2012. Spatial distribution of glacial erosion rates in the St. Elias range, Alaska, inferred from a realistic model of glacier dynamics. J. Geophys. Res. 117: F03027. doi:10.1029/2011JF002291.

Headley, R. M.; Enkelmann, E.; and Hallet, B. 2013. Examination of the interplay between glacial processes and exhumation in the Saint Elias Mountains, Alaska. Geosphere 9:229–241.

Hogan, L. G.; Scheidegger, K. F.; Kulm, L. D.; Dymond, J.; and Mikkelsen, N. 1978. Biostratigraphic and tectonic implications of ^{40}Ar-^{39}Ar dates of ash layers from the northeast Gulf of Alaska. Geol. Soc. Am. Bull. 89:1259–1264.

Hoskin, P. W. O. 2003. The composition of zircon and igneous and metamorphic petrogenesis. *In* Hanchar, J. M., and Hoskin, P. W. O., eds. Zircon. Rev. Mineral. Geochem. 53:27–62.

Huber, B.; Bahlburg, H.; and Pfänder, J. A. 2018. Single grain heavy mineral provenance of garnet and amphibole in the Surveyor Fan and precursor sediments on the Gulf of Alaska abyssal plain—implications for climate-tectonic interactions in the St. Elias orogen. Sediment. Geol. 372: 173–192.

Hudson, T., and Plafker, G. 1982. Paleogene metamorphism of an accretionary flysch terrane, eastern Gulf of Alaska. Geol. Soc. Am. Bull. 93:1280–1290.

Hurford, A. J., and Carter, A. 1991. The role of fission track dating in discrimination of provenance. *In* Morton, A. C.; Todd, S. P.; and Haughton, P. D. W., eds. Developments in sedimentary provenance studies. Geol. Soc. Lond. Spec. Publ. 57:67–78.

Ingle, J. C., Jr. 1973. Summary comments on Neogene biostratigraphy, physical stratigraphy, and paleo-oceanography in the marginal northeastern Pacific Ocean Deep Sea Drilling Project, Leg 18. *In* Musich, L. F., and Weser, O. E., eds. Initial reports of the Deep Sea Drilling Project. Vol. 18, Washington, DC, Government Printing Office, p. 949–960.

Jaeger, J. M.; Gulick, S.; LeVay, L. J.; Asahi, H.; Bahlburg, H.; Belanger, C. L.; Berbel, G.; et al. 2014. Methods. *In* Jaeger, J. M.; Gulick, S.; LeVay, L. J.; and the Expedition 341 Scientists, eds. Expedition 341 reports: southern Alaska margin. Proc. Integrated Ocean Drilling Pro-

gram, vol. 341. College Station, TX, Integrated Ocean Drilling Program. doi:10.2204/iodp.proc.341.102.2014.
Kinny, P. D., and Maas, R. 2003. Lu-Hf and Sm-Nd isotope systems in zircon. *In* Hanchar, J. M., and Hoskin, P. W. O., eds. Zircon. Rev. Mineral. Geochem. 53:327–341.
Koschek, G. 1993. Origin and significance of the SEM cathodoluminescence from zircon. J. Microsc. 171:223–232.
Lagoe, M. B.; Eyles, C. H.; Eyles, N.; and Hale, C. 1993. Timing of late Cenozoic tidewater glaciation in the far North Pacific. Geol. Soc. Am. Bull. 105:1542–1560.
Lagoe, M. B., and Zellers, S. D. 1996. Depositional and microfaunal response to Pliocene climate change and tectonics in the eastern Gulf of Alaska. Mar. Micropaleontol. 27:121–140.
Madsen, J. K.; Thorkelson, D. J.; Friedman, R. M.; and Marshall, D. D. 2006. Cenozoic to Recent plate configurations in the Pacific Basin: ridge subduction and slab window magmatism in western North America. Geosphere 2:11–34.
Mahoney, J. B.; Gordee, S. M.; Haggart, J. W.; Friedman, R. M.; Diakow, L. J.; and Woodsworth, G. J. 2009. Magmatic evolution of the eastern Coast Plutonic Complex, Bella Coola region, west-central British Columbia. Geol. Soc. Am. Bull. 121:1362–1380.
Manley, W. F., and Kaufman, D. S. 2002. Alaska Paleo-Glacier Atlas. Institute of Arctic and Alpine Research (INSTAAR), University of Colorado. http://instaar.colorado.edu/QGISL/ak_paleoglacier_atlas.
Mann, D. H., and Hamilton, T. D. 1995. Late Pleistocene and Holocene paleoenvironments of the North Pacific coast. Quat. Sci. Rev. 14:449–471.
Meigs, A.; Johnston, S.; Garver, J.; and Spotila, J. 2008. Crustal-scale structural architecture, shortening, and exhumation of an active, eroding orogenic wedge (Chugach/St. Elias Range, southern Alaska). Tectonics 27: TC4003. doi:10.1029/2007TC002168.
Mendenhall, W. C. 1905. Geology of the central Copper River region, Alaska. U.S. Gel. Surv. Prof. Pap. 41, 170 p.
Moecher, D. P., and Samson, S. D. 2006. Differential zircon fertility of source terranes and natural bias in the detrital zircon record: implications for sedimentary provenance analysis. Earth Planet. Sci. Lett. 247:252–266.
Molnia, B. 2008. Glaciers of North America. Alaska. *In* Williams, R. S., Jr., and Ferrigno, J. G., eds. Satellite image atlas of glaciers of the world. U.S. Geol. Surv. Prof. Pap. 1386-K, 525 p.
Montelli, A.; Gulick, S. P. S.; Worthington, L. L.; Mix, A.; Davies-Walczak, M.; Zellers, S. D.; and Jaeger, J. M. 2017. Late Quaternary glacial dynamics and sedimentation variability in the Bering Trough, Gulf of Alaska. Geology 45:251–254.
Moore, J. C.; Byrne, T.; Plumley, P. W.; Reid, M.; Gibbons, H.; and Coe, R. S. 1983. Paleogene evolution of the Kodiak Islands, Alaska: consequences of ridge-trench interaction in a more southerly latitude. Tectonics 2: 265–293.
Ness, G. E., and Kulm, L. D. 1973. Origin and development of Surveyor Deep-Sea Channel. Geol. Soc. Am. Bull. 84: 3339–3354.
O'Sullivan, G. J.; Chew, D. M.; and Samson, S. D. 2016. Detecting magma-poor orogens in the detrital record. Geology 44:871–874.
O'Sullivan, P. B., and Currie, L. D. 1996. Thermotectonic history of Mt Logan, Yukon Territory, Canada: implications of multiple episodes of Middle to Late Cenozoic denudation. Earth Planet. Sci. Lett. 144:251–261.
Pavlis, T. L.; Chapman, J. B.; Bruhn, R. L.; Ridgway, K.; Worthington, L. L.; Gulick, S. P. S.; and Spotila, J. 2012. Structure of the actively deforming fold-thrust belt of the St. Elias orogen with implications for glacial exhumation and three-dimensional tectonic processes. Geosphere 8:991–1019.
Pavlis, T. L., and Sisson, V. B. 1995. Structural history of the Chugach metamorphic complex in the Tana River region, eastern Alaska: a record of Eocene ridge subduction. Geol. Soc. Am. Bull. 107:1333–1355.
Perry, S. E.; Garver, J. I.; and Ridgway, K. D. 2009. Transport of the Yakutat terrane, southern Alaska: evidence from sediment petrology and detrital zircon fission-track and U/Pb double dating. J. Geol. 117:156–173.
Pewé, T. L. 1975. Quaternary geology of Alaska. U.S. Geol. Surv. Prof. Pap. 835, 145 p.
Plafker, G. 1987. Regional geology and petroleum potential of the northern Gulf of Alaska continental margin. *In* Scholl, D. W.; Grantz, A.; and Vedder, J. G., eds. Geology and resource potential of the continental margin of western North America and adjacent ocean basins—Beaufort Sea to Baja California. Earth Sci. Ser., vol. 6. Menlo Park, CA, Circum-Pacific Council for Energy and Mineral Resources, p. 229–268.
Plafker, G.; Moore, J. C.; and Winkler, G. R. 1994. Geology of the southern Alaska margin. *In* Plafker, G., and Berg, H. C., eds. The geology of Alaska (Geology of North America, Vol. G-1). Boulder, CO, Geol. Soc. Am., p. 389–449.
Post, A. 1972. Periodic surge origin of folded medial moraines on Bering piedmont glacier, Alaska. J. Glaciol. 11:219–226.
Rahl, J. M.; Reiners, P. W.; Campbell, I. H.; Nicolescu, S.; and Allen, C. M. 2003. Combined single-grain (U-Th)/He and U/Pb dating of detrital zircons from the Navajo Sandstone, Utah. Geology 31:761–764.
Rea, D. K., and Snoeckx, H. 1995. Sediment fluxes in the Gulf of Alaska: paleoceanographic record from Site 887 on the Patton-Murray Seamount platform. *In* Rea, D. K.; Basov, I. A.; Scholl, D. W.; and Allan, J. F., eds. Proc. Ocean Drilling Program, scientific results, vol. 145. College Station, TX, Ocean Drilling Program, p. 247–256. doi:10.2973/odp.proc.sr.145.122.1995.
Reece, R. S.; Gulick, S. P. S.; Horton, B. K.; Christeson, G. L.; and Worthington, L. L. 2011. Tectonic and climatic influence on the evolution of the Surveyor Fan and Channel system, Gulf of Alaska. Geosphere 7:830–844.
Reiners, P. W. 2005. Zircon (U-Th)/He thermochronometry. *In* Reiners, P. W., and Ehlers, T. A., eds. Low-temperature thermochronology: techniques, interpretations, and applications. Rev. Mineral. Geochem. 58: 151–179.

Reiners, P. W., and Brandon, M. T. 2006. Using thermochronology to understand orogenic erosion. Annu. Rev. Earth Planet. Sci. 34:419–466.

Roig, C. 2014. Oxygen and hafnium isotope geochemistry of zircon, quartz, and garnet from the Crawfish Inlet and Krestof plutons, Baranof Island, Alaska. *In* Varga, R. J., ed. Keck Geology Consortium Undergraduate Research Symposium, 27th (South Hadley, MA), Proc. Claremont, CA, Geol. Dept., Pomona College, 6 p.

Rowley, D. B.; Xue, F.; Tucker, R. D.; Peng, Z. X.; Baker, J.; and Davis, A. M. 1997. Ages of ultrahigh pressure metamorphism and protolith orthogneisses from the eastern Dabie Shan: U/Pb zircon geochronology. Earth Planet. Sci. Lett. 151(3–4):191–203.

Rubatto, D. 2017. Zircon: the metamorphic mineral. *In* Kohn, M. J.; Engi, M.; and Lanari, P., eds. Petrochronology: methods and applications. Rev. Mineral. Geochem. 83:261–295.

Schneider, E.; Garver, J. I.; and Davidson, C. 2015. Cooling history of the Sanak-Baranof plutons, Alaska, using zircon and apatite (U-Th)/He thermochronology. Geol. Soc. Am. Abstr. Program 47(4):58.

Siebel, W., and van den Haute, P. 2009. Radiometric dating and tracing. *In* Nagy, S., ed. Radiochemistry and nuclear chemistry, vol. 1. Encyclopedia of Life Support Systems. Oxford, EOLSS, p. 157–196.

Sisson, V. B.; Hollister, L. S.; and Onstott, T. C. 1989. Petrologic and age constraints on the origin of a low-pressure/high-temperature metamorphic complex, southern Alaska. J. Geophys. Res. 94:4392–4410.

Sisson, V. B.; Poole, A. R.; Harris, N. R.; Burner, H. C.; Pavlis, T. L.; Copeland, P.; Donelick, R. A.; and McLelland, W. C. 2003. Geochemical and geochronologic constraints for genesis of a tonalite-trondjemite suite and associated mafic intrusive rocks in the eastern Chugach Mountains, Alaska: a record of ridge-transform subduction. *In* Sisson, V. B.; Roeske, S. M.; and Pavlis, T. L., eds. Geology of a transpressional orogen developed during ridge-trench interaction along the North Pacific margin. Geol. Soc. Am. Spec. Pap. 371:293–326.

Spotila, J. A., and Berger, A. L. 2010. Exhumation at orogenic indentor corners under long-term glacial conditions: example of the St. Elias orogen, southern Alaska. Tectonophysics 490:241–256.

Spotila, J. A.; Buscher, J. T.; Meigs, A. J.; and Reiners, P. W. 2004. Long-term glacial erosion of active mountain belts: example of the Chugach–St. Elias Range, Alaska. Geology 32:501–504.

Stevenson, A. J., and Embley, R. 1987. Deep-sea fan bodies, terrigenous turbidite sedimentation and petroleum geology, Gulf of Alaska. *In* Scholl, D. W.; Grantz, A.; and Vedder, J. G., eds. Geology and resource potential of the continental margin of western North America and adjacent ocean basins—Beaufort Sea to Baja California. Earth Sci. Ser., vol. 6. Menlo Park, CA, Circum-Pacific Council for Energy and Mineral Resources, p. 503–522.

Tomkin, J. H., and Roe, G. H. 2007. Climate and tectonic controls on glaciated critical-taper orogens. Earth Planet. Sci. Lett. 262:385–397.

Vermeesch, P. 2012. On the visualisation of detrital age distributions. Chem. Geol. 312–313:190–194.

Vermeesch, P.; Resentini, A.; and Garzanti, E. 2016. An R package for statistical provenance analysis. Sediment. Geol. 336:14–25.

Vervoort, J. D.; Patchett, P.; Blichert-Toft, J.; and Albarède, F. 1999. Relationships between Lu-Hf and Sm-Nd isotopic systems in the global sedimentary system. Earth Planet. Sci. Lett. 168:79–99.

White, T.; Bradley, D.; Haeussler, P.; and Rowley, D. B. 2017. Late Paleocene–early Eocene paleosols and a new measure of the transport distance of Alaska's Yakutat Terrane. J. Geol. 125(2):113–123.

Worthington, L. L.; Daigle, H.; Clary, W. A.; Gulick, S. P. S.; and Montelli, A. 2018. High sedimentation rates and thrust fault modulation: insights from ocean drilling offshore the St. Elias Mountains, southern Alaska. Earth Planet. Sci. Lett. 483:1–12.

Worthington, L. L.; Gulick, S. P. S.; and Pavlis, T. L. 2010. Coupled stratigraphic and structural evolution of a glaciated orogenic wedge, offshore St. Elias orogen, Alaska. Tectonics 29:TC6013. doi:10.1029/2010TC002723.

Worthington, L. L.; Van Avendonk, H. J. A.; Gulick, S. P. S.; Christeson, G. L.; and Pavlis, T. L. 2012. Crustal structure of the Yakutat terrane and the evolution of subduction and collision in southern Alaska. J. Geophys. Res. 117:B01102. doi:10.1029/2011JB008493.